ADVANCED HEALTHCARE MATERIALS
www.advhealthmat.de

Study of the Structure of Hyperbranched Polyglycerol Coatings and Their Antibiofouling and Antithrombotic Applications

Eli Moore, Alexander J. Robson, Amy R. Crisp, Michaelia P. Cockshell, Anouck L. S. Burzava, Raja Ganesan, Nirmal Robinson, Sameer Al-Bataineh, Victoria Nankivell, Lauren Sandeman, Markus Tondl, Glen Benveniste, John W. Finnie, Peter J. Psaltis, Laurine Martocq, Alessio Quadrelli, Samuel P. Jarvis, Craig Williams, Gordon Ramage, Ihtesham U. Rehman, Christina A. Bursill, Tony Simula, Nicolas H. Voelcker, Hans J. Griesser, Robert D Short, and Claudine S. Bonder**

While blood-contacting materials are widely deployed in medicine in vascular stents, catheters, and cannulas, devices fail in situ because of thrombosis and restenosis. Furthermore, microbial attachment and biofilm formation is not an uncommon problem for medical devices. Even incremental improvements in hemocompatible materials can provide significant benefits for patients in terms of safety and patency as well as substantial cost savings. Herein, a novel but simple strategy is described for coating a range of medical materials, that can be applied to objects of complex geometry, involving plasma-grafting of an ultrathin hyperbranched polyglycerol coating (HPG). Plasma activation creates highly reactive surface oxygen moieties that readily react with glycidol. Irrespective of the substrate, coatings are uniform and pinhole free, comprising O—C—O repeats, with HPG chains packing in a fashion that holds reversibly binding proteins at the coating surface. In vitro assays with planar test samples show that HPG prevents platelet adhesion and activation, as well as reducing (>3 log) bacterial attachment and preventing biofilm formation. Ex vivo and preclinical studies show that HPG-coated nitinol stents do not elicit thrombosis or restenosis, nor complement or neutrophil activation. Subcutaneous implantation of HPG coated disks under the skin of mice shows no evidence of toxicity nor inflammation.

1. Introduction

All implanted materials elicit some level of foreign-body-response and carry an associated risk, even where materials meet current biocompatibility standards.[1] This is particularly the case for blood-contacting materials. The introduction of vascular stents has provided surgeons with significant and meaningful tools in the fight against the ever-increasing epidemic that is cardiovascular disease (CVD).[2] Indeed, CVDs are the leading cause of death globally causing an estimated 18 million deaths per year (2019 numbers).[3,4] The ability to physically reopen and maintain patency in diseased and occluded vasculature has saved countless lives. Furthermore, generational refinements in design have resulted in significant improvements in the safety and patency of vascular stents.[5] However, two significant challenges remain: i) exposure of the stents to blood results in the rapid adsorption and adhesion of proteins and cells, initiating a cascade of events that can

E. Moore, M. P. Cockshell, R. Ganesan, N. Robinson, M. Tondl, C. S. Bonder
Centre for Cancer Biology
University of South Australia and SA Pathology
Adelaide, South Australia 5000, Australia
E-mail: Claudine.Bonder@unisa.edu.au

The ORCID identification number(s) for the author(s) of this article can be found under https://doi.org/10.1002/adhm.202401545

DOI: 10.1002/adhm.202401545

A. J. Robson, R. D Short
Department of Chemistry
The University of Sheffield
Dainton Building
Brook Hill
Sheffield S3 7HF, UK
E-mail: a.j.robson@sheffield.ac.uk

A. R. Crisp, L. Martocq
School of Engineering
Lancaster University
Lancaster LA1 4YW, UK

A. L. S. Burzava, H. J. Griesser
Future Industries Institute
University of South Australia
Mawson Lakes, South Australia 5095, Australia

lead to stent thrombosis (ST); ii) In-stent restenosis (ISR), an immune-triggered complication leading to vessel reocclusion.

ST can be a life-threatening complication, often requiring emergency intervention, which can also lead to amputations or death. The challenge is to prevent platelet adhesion, activation and thrombus formation.[6] While the physiological processes that give rise to thrombosis in stents are well understood and have been documented for decades,[7] suitable material engineering solutions to mitigate these complex and highly evolved processes have not been developed.

Current best practice following implantation of vascular stents includes the long-term prescription of antiplatelet, blood-thinning medications to reduce the likelihood of ST. As with many pharmacological approaches, the administration of dual antiplatelet therapy (DAPT) for durations of several months to years can have serious side effects, including upper gastrointestinal bleeding, ecchymosis, hematuria, and epistaxis, resulting in greatly reduced quality of life for patients.[8,9] The ongoing use of DAPT also makes follow-up and emergency procedures potentially fatal due to the high risk of increased bleeding during surgery. However, patients who cease antiplatelet medications early, e.g., to perform scheduled surgery, have an elevated risk of ST and perioperative myocardial infarction.[10,11]

ISR is an immune-triggered complication leading to vessel reocclusion, that develops over months, requiring further intervention and possibly surgery.[12–14] This is particularly evident in peripheral arterial disease where reported rates of ISR have been as high as 40% in some patient populations in the first 12 months after treatment with a stent.[15–17] After initial vascular injury resulting from stent insertion, inflammatory factors are released by several cell types including platelets, macrophages and lymphocytes.[18] These factors lead to the secretion of growth factors that increases the proliferation and migration of vascular smooth muscle cells into the intimal region, leading to intimal hyperplasia and ISR.[19,20]

Drug-eluting stents (DES) have been the industry's solution to this problem, with cellular proliferation put on hold for as long as the drug continues to leach from the stent. This approach has had varied levels of success, and is considered the gold standard at present, but is limited by the finite therapeutic load a device can deliver.[21] Exposed stent struts and polymer coatings, that act as reservoirs for the drug, can also trigger late thrombotic events after the therapeutic window has expired.[22] There have also been reports of higher rates of all-cause mortality and amputations in patients with peripheral arterial disease treated with paclitaxel-coated devices, compared with uncoated devices.[23–25]

Thrombosis and restenosis are challenges in a broader range of blood contacting materials, including central venous catheters (CVCs) where additional challenges arise from catheter-related bloodstream infections (CRBSIs), which are difficult and costly to treat as well as ultimately potentially lethal.[26] CVCs are a common route of systemic infection by bacterial strains, such as *Staphylococcus epidermidis* that exist harmlessly on the skin surface, but upon entering the blood stream result in device colonization by forming biofilms.[27] In clinical practice, the occurrence of a CVC infection will worsen the patient's prognosis, reduce treatment options, and increase the patient's overall hospital stay. When a CVC infection involves a mature biofilm, the mortality rate becomes exponentially greater because biofilms are 1000 times more resistant to antibiotic treatment than planktonic derived infections.[28] Every year, in the US, there are 250 000–400 000 reported cases of CRBSIs with an associated mortality rate of 12%–15%.[29,30] The National Biofilms Innovation Centre (NBIC) report that as of 2019 $387 bn is spent globally dealing with the consequences of biofilms in hospital acquired infections, of which $11.5 bn is estimated to be due to CVC related infections.[31]

In blood-contacting materials, the two primary challenges of hemocompatibility and infection prevention have a common "solution": the prevention of cell attachment through minimization of nonspecific protein binding.[32,33] Initial protein adsorption to the surface of an implantable material leads to complications, such as chronic infection and thrombosis.[34] In this context, novel coating technologies have been intensively investigated to provide new surfaces that prevent, or minimize, protein, and cell binding, including organic polymers, inorganic films, and the use of biological components.[35–38]

N. Robinson, J. W. Finnie, P. J. Psaltis, C. S. Bonder
Adelaide Medical School
University of Adelaide
Adelaide, South Australia 5000, Australia

S. Al-Bataineh, T. Simula
TekCyte Limited
Mawson Lakes, South Australia 5095, Australia

V. Nankivell, L. Sandeman, P. J. Psaltis, C. A. Bursill
Vascular Research Centre
Heart and Vascular Program
Lifelong Health Theme
South Australian Health and Medical Research Institute
Adelaide, South Australia 5000, Australia

G. Benveniste
Ashford Vascular
Ashford, South Australia 5035, Australia

P. J. Psaltis
Department of Cardiology
Central Adelaide Local Health Network
Adelaide, South Australia 5000, Australia

A. Quadrelli, S. P. Jarvis
Department of Physics
Lancaster University
Lancaster LA1 4YB, UK

C. Williams
Microbiology Department
Royal Lancaster Infirmary
Lancaster LA1 4RP, UK

G. Ramage
Department of Nursing and Community Health
Glasgow Caledonian University
Glasgow G4 0BA, UK

I. U. Rehman
School of Medicine
University of Central Lancashire
Preston PR1 2HE, UK

N. H. Voelcker
Monash Institute of Pharmaceutical Sciences
Monash University
Parkville, Victoria 3052, Australia

N. H. Voelcker
Melbourne Centre for Nanofabrication
Victorian Node of the Australian National Fabrication Facility
Clayton, Victoria 3168, Australia

The main challenge in developing coatings for medical devices lies in striking a balance between an implementable, effective and scalable production method and achieving optimal coating properties for the intended biological environment. Polyethylene oxide (PEO)-like surfaces, which boast a repeat C—O—C moiety, are one of the most common coatings used in biomaterials because they are naturally antifouling, hydrophilic, and nonbiodegradable.[39] These materials are widely accepted and repeatedly demonstrated as nonfouling because they increase surface hydrophilicity, which prevents proteins from displacing preadsorbed water.[40]

Polyethylene glycol (PEG) has long remained the gold standard in nonfouling coatings for medical devices showing high biocompatibility and minimization of protein adsorption.[41] However, these coatings suffer low thermal stability and high levels of oxidative degradation causing a reduction in nonfouling capabilities over time.[34,41,42] Hyperbranched polymer coatings, such as hyperbranched polyglycerol (HPG) have been the source of intense interest since 1990 due to their uniform surface coverage, improved thermal, and oxidative stability, as well as enhanced protein repulsion.[41,43–45] These materials have applications that span from preventing implant failure, due to antifouling and anticoagulant properties, to drug delivery systems where HPG is used to prevent nanoparticle coagulation.[46–48] HPG has consistently been shown as highly biocompatible and resistant to proteins.[49] Long-term storage stability of HPG coatings has also been demonstrated, a vital requirement for industrial application.[33]

Routes to HPG formation have been explored via both cationic and anionic ring opening, using graft-to and graft-from approaches to coat a myriad of materials from metal and silicon to clinically relevant polymers.[44,45,50,51] HPG is accessible through a one-step synthesis using an anionic ring opening mechanism.[52] These approaches often evidence the production of a HPG coating, using an initiator molecule, in the range of 5–25 nm in thickness, on a single class of substrate materials.[41,53–55] The initiator attacks the glycidol monomer, producing a secondary alkoxide, which in turn can attack further glycidol monomers. Rapid proton exchange between different chain ends (primary and secondary alcohols) results in the formation of a branched structure, with the reaction continuing until all monomer has reacted, or the process is terminated by quenching the process to neutralize the alkoxides.[56] Wet chemistry approaches are favored within the literature; however, these methods are flawed by extensive and complex protocols that require slow monomer addition to the catalyst/initiator under a controlled environment, before washing and refining the HPG product to affix to the desired material.[57] Graft-from approaches rely on deprotonation of the target material surface to promote self-initiation in glycidol which will lead to a covalently bonded HPG coating.[45] This approach naturally forms a more uniform and consistent surface coating, arguably further reducing protein adsorption.[53,54] However, chemical deprotonation techniques are inapplicable across a broad range of substrate materials.[45]

An alternative approach using plasma activation, generating an oxide layer to promote grafting, is applicable to a more diverse range of materials without the production of chemical waste.[32,58] Plasma has the distinctive advantage of being an immersive technique, activating all surfaces of an object (e.g., a vascular stent) within the plasma, as well as having proven scalability. A plasma activation-based protocol was recently optimized by Burzava et al. where polystyrene (PS) on Si was exposed to air plasma (100 W, 5 min) before immediate submersion in glycidol (100 °C, 24 h), providing a coating of 24 nm thickness.[32]

In spite of the extensive exploration of coating production methods there is notably a distinct absence of chemical compositional characterization and frequently water contact angle is the only evidence provided to prove the HPG coating has formed.[57,59,60] Surface analysis is vital for antibiofouling coatings because issues arise where a surface coating is not pinhole free.[61]

Herein, we report on the deposition, structure, and properties of a novel protocol to produce ultrathin HPG coatings on a wide range of materials and demonstrate both antithrombotic and antibiofouling properties (**Figure 1**). We show our protocol, which utilizes plasma to rapidly and uniformly activate the substrate, yields an ultrathin HPG coating that is tightly bound and pin-hole free irrespective of the substrate. The various stages of coating preparation are rigorously evaluated by X-ray photoelectron spectroscopy (XPS) to better understand the process leading to coating formation and the resultant chemical structure. Antibiofouling properties are explored through single protein adsorption experiments and direct culture with several microorganisms commonly associated with device colonization. Using XPS gas-cluster ion milling, we demonstrate that any attaching proteins are held at the coating/biological interface and do not penetrate the HPG coating. We have used the novel approach of Fourier-transform infra-red (FTIR spectroscopy to show that the HPG coating effectively prevents the transition of microorganisms from planktonic to biofilm. Ex vivo studies, using isolated platelets and fresh human blood (allowing us to minimize the amount of heparin added and therefore reduce pharmacological effects), demonstrate that our HPG coating is highly effective at preventing the binding and activation of platelets and greatly reducing the thrombogenicity of a range of substrates including nitinol stents. Using the gold standard apolipoprotein E (*ApoE*) knockout atherosclerotic mouse model, we demonstrate that HPG-coated stainless-steel (SS) stents exhibit significantly reduced restenosis and remained patent after 28 days, while, in stark contrast, a majority of control stents became completely occluded.

2. Results and Discussion

2.1. Surface Analysis of HPG Coating and Coating Process

2.1.1. XPS Analysis of Substrate Materials

Analysis of the HPG grafting process was performed on titanium coated silicon wafer (TiSi), and polytetrafluoroethylene (PTFE) substrates, selected due to their clinical relevance and ease of use with surface analysis techniques. For each substrate, preliminary XPS evaluation was carried out to determine the baseline chemical composition.

To form the TiSi substrate, Si wafer was sputter coated with Ti, forming a uniform coating of 40 ± 5 nm. XPS of TiSi reveals carbon (C), oxygen (O), Ti, calcium (Ca), and nitrogen (N)

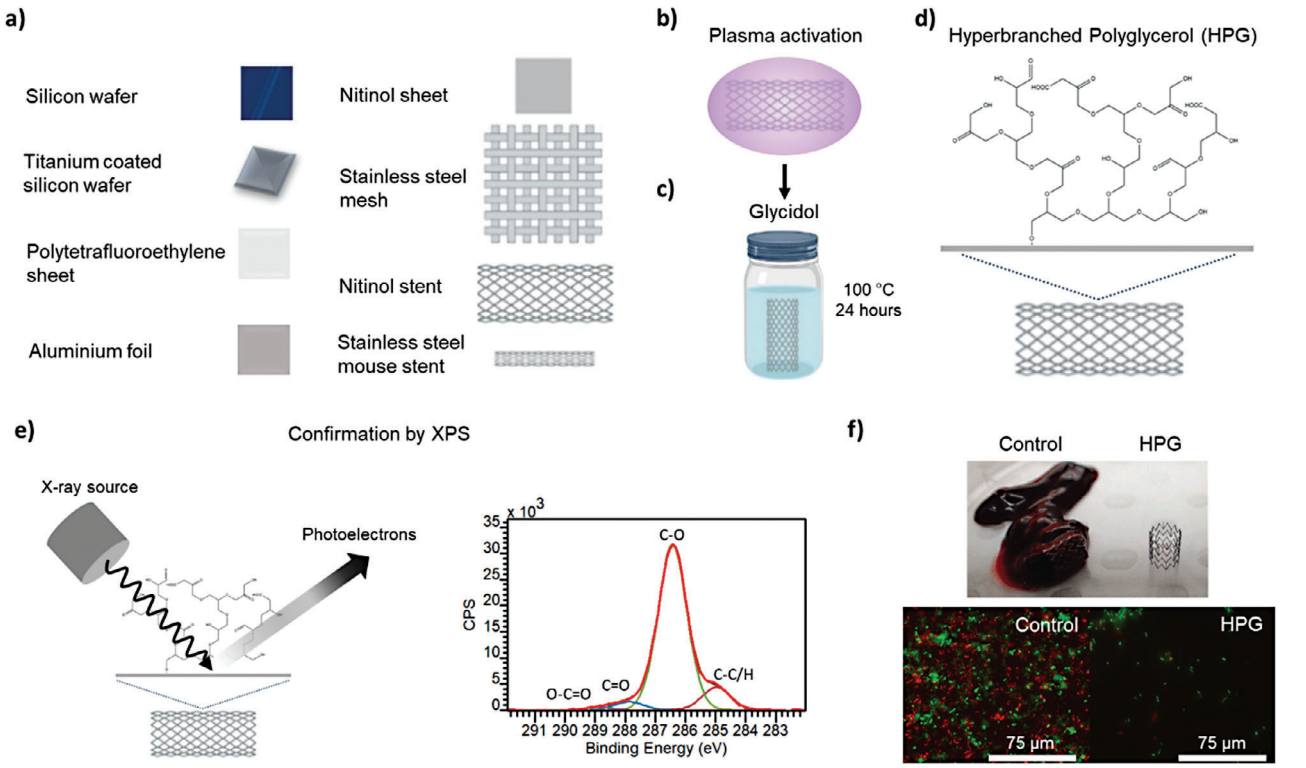

Figure 1. Graphical overview of HPG coating process. a) Different materials were successfully coated with HPG. b) The first step of process is activating the material with plasma followed by c) incubation in glycidol at 80–100 °C for 24 h leading to the d) growth of a nanometers-thin layer of HPG. e) Successful HPG coating was confirmed by XPS. f) HPG is evidenced to resist whole blood adhesion and bacterial biofilms.

signals (**Figure** 2a). The amount of C detected (41.3% of the elemental composition) indicates the presence surface hydrocarbon (HC) contamination. The Ti 2p spectrum contains two peaks at 458.66 and 464.28 eV, corresponding to the Ti $2p^{3/2}$ and $2p^{1/2}$ environments, respectively (Figure S1, Supporting Information). The positions of these signals are consistent with Ti(IV) oxide (TiO_2), with a small contribution (13.3% of the Ti 2p signal) from Ti metal, Ti(II) and Ti(III).[62] The O 1s (Figure 2c) reveals three binding environments: two at 529.9 and 531.3 eV assigned to Ti—O—Ti and Ti—O—H, respectively,[63] and a third at and 532.5 eV assigned to C—O. The absence of any signal from Si indicates that the surface TiO_2 layer is thicker than the XPS sampling depth.

PTFE was chosen as an example of a clinically relevant polymer, widely used in medical devices.[64] XPS analysis of PTFE wide scan spectra (**Figure** 3a) show predominantly C and F signals, with a low (<0.5%) amount of O, indicating negligible surface oxidation. The C 1s core line spectrum (Figure 3b) shows a strong signal at 292 eV, consistent with the CF_2 environment. A further trace signal at 285 eV indicates a low level of HC contamination. The O 1s core line spectrum (Figure 3c) is centered at 532.6 eV corresponds to C—O, likely due to surface HC contamination.

2.1.2. XPS Analysis of Plasma Activated Substrate

The protocol for fabricating HPG coatings requires plasma activation of the substrate with an air plasma for 20 min prior to immersion in distilled glycidol. In order to better understand the grafting process, substrates were analyzed with XPS after the plasma activation step, but before exposure to glycidol.

In plasma-activated TiSi (Figure 2d–f; and Figure S1b, Supporting Information), removal of HC contamination is clearly evident (C drops from 41.3% to 6.2%). Trace amounts of Si are detected, attributed to contamination from the plasma reactor. O can be seen to increase from 39.9% in the original TiSi wafer to 64.5%, in line with the objective of incorporating reactive surface moieties that facilitate the surface grafting of glycidol. The Ti $2p^{1/2}$ and $2p^{3/2}$ binding energy positions remain relatively unchanged (Figure S1, Supporting Information), with only minor changes detected in the line shape, indicating a very slight increase in Ti(IV) from 86.7% to 87.5% of the Ti2p signal. Compared to the original TiSi substrate, the O:Ti ratio marginally increases from 2.3:1 to 2.7:1 following plasma activation. Plasma activation also resulted in an additional O 1s binding environment at 532.85 eV (Figure 2f), which, based on previous literature and the removal of HC contamination, we postulate as Ti—O—O dangling bonds.[63] The Ti—OH and Ti—O—O moieties are potentially highly reactive sites that would facilitate the radical grafting of glycidol, initiating the polymerization process and growth of HPG coatings.

Plasma activation of PTFE (Figure 3d–f; and Figure S2b, Supporting Information) results in a small increase in O (from 0.4% to 2.9%). C 1s peak fitting reveals a number of new carbon environments, clearly identifiable between 285 and 292 eV; these are anticipated with the introduction of oxygen binding environments (such as C—O, C═O, etc.), as well as potential damage to

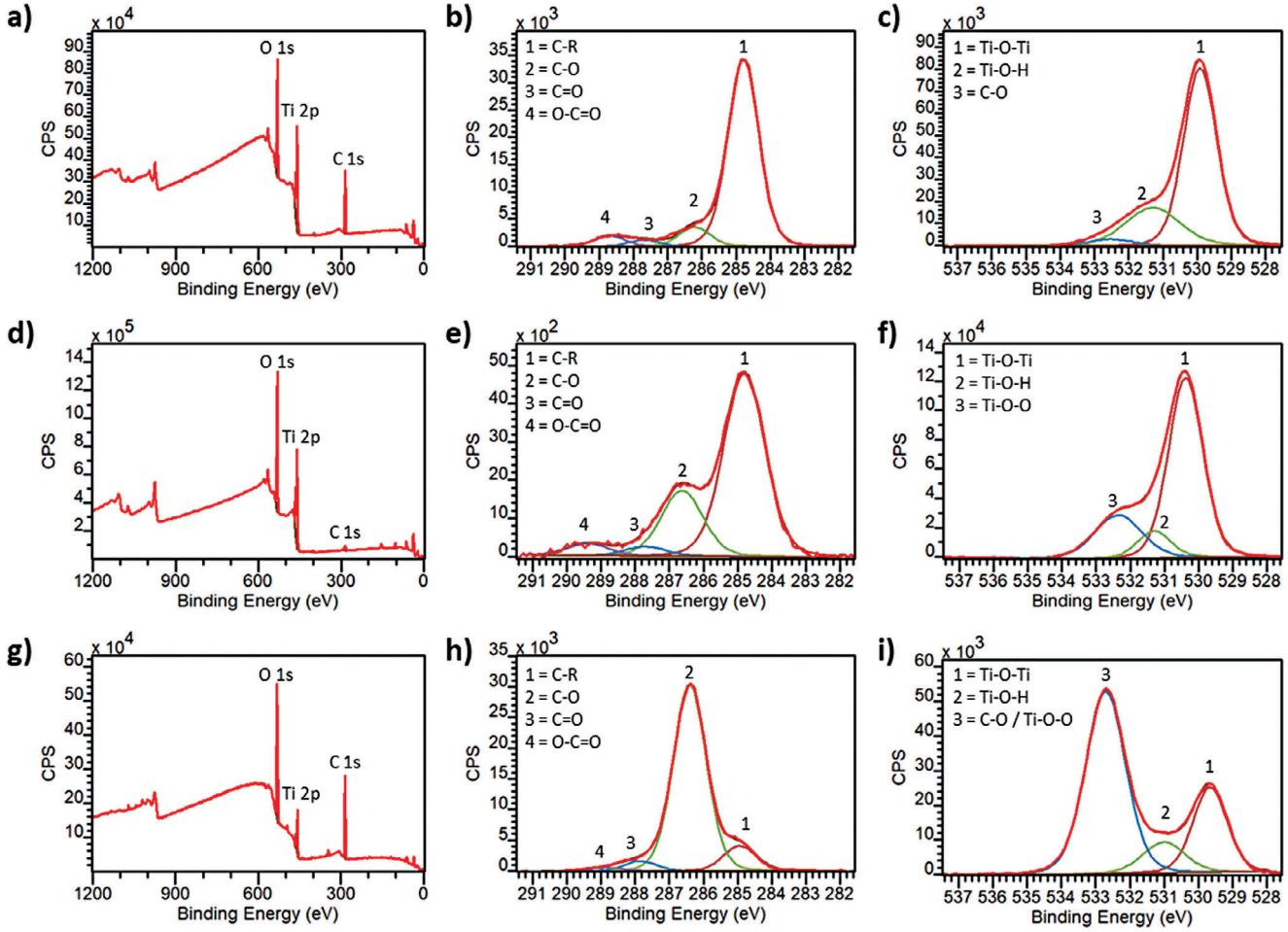

Figure 2. XPS spectra of TiSi substrate throughout the HPG grafting process. a–c) Clean TiSi wafer prior to the HPG process. d–f) TiSi substate after plasma activation, but before HPG grafting. g–i) TiSi substate after HPG grafting. Wide scan spectrum displaying chemical composition of the coating a,d,g). C 1s core line spectra b,e,h). O 1s core line spectra c,f,i). Associated Ti 2p spectra shown in Figure S1 (Supporting Information). Composition % values shown in Table S1 (Supporting Information).

the CF_2 backbone structure, resulting in a broad range of carbon-fluorine-oxygen environments (potential binding environments are labeled on Figure 3e). The O 1s spectrum centers around 535 eV, likely corresponding to O—C—F_n environments.[65] Similar to plasma activated TiSi, these O—C—F_n environments are potentially reactive sites which facilitate the HPG grafting process.

2.1.3. Analysis of HPG Grafting on Substrate

Following plasma activation of the substrate, substrates were immersed in distilled glycidol and left to polymerize in an oven at 80 °C for 24 h. Polymerization was terminated by removing the unreacted monomer solution and quenching the reaction by a succession of methanol washes.

XPS analysis of glycidol grafted to the various (activated) substrate materials reveals remarkably chemically similar HPG coatings (Figures 2g–i and 3g–i). The XPS wide scan taken for HPG on TiSi (Figure 2h) reveals an increased C signal (49.7%, compared to 6.2% in plasma activated TiSi), indicating deposition of a coating. Clearly identifiable Ti 2p peaks indicate the thinness of the coating, less than the XPS sampling depth of 5–10 nm.[66] The C 1s core line spectrum (Figure 2h) reveals a characteristically high C—O signal (81.4% of the C 1s signal) at 286.4 eV, indicative of the high C—O—C content and the successful formation of HPG. Nevertheless, the "true" C—O—C content of the HPG may be higher than measured by XPS, because the C—H/R contributions, usually attributed to HC contamination, could in this instance be located at the TiSi substrate (i.e., not removed by plasma activation or contamination between plasma activation and immersion in glycidol). Observation of this potential substrate HC contamination is a result of the ultrathin nature of the HPG coating. In the O 1s (Figure 2i), a strong peak emerges at 532.7 eV (67.6% of the O 1s signal) originating from C—O—C, in correlation with the C 1s C—O peak, and potentially Ti—O—O from the Ti—Si substrate.

The XPS spectra recorded for HPG coated PTFE (Figure 3g–i) again show clear signs of HPG coating. The wide scan spectrum (Figure 3g) shows a small increase in C compared to the plasma activated sample (from 35.6% in plasma activated PTFE to 43.6% in the HPG coated sample), but a much greater increase in O (from 2.9% to 15.7%), again indicative of coating formation.

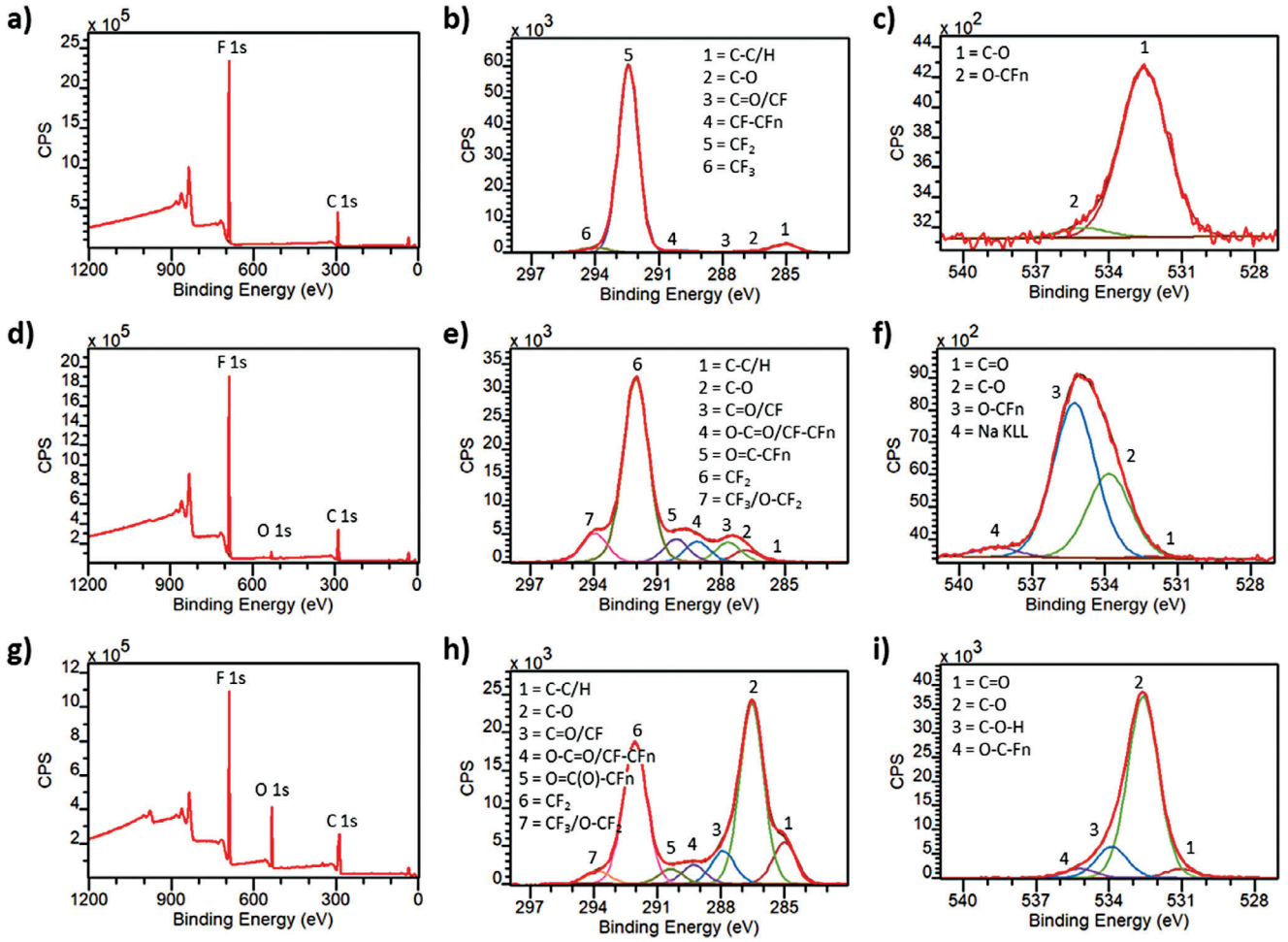

Figure 3. XPS spectra of PTFE substrate throughout the HPG grafting process. a–c) Clean PTFE prior to the HPG process. d–f) PTFE substrate after plasma activation, but before HPG grafting. g–i) PTFE substate after HPG grafting. Wide scan spectrum displaying chemical composition of the coating a,d,g). C 1s core line spectra b,e,h). Note that while several potential environments are labeled, a range of other C/F/O environments may be present. O 1s core line spectra c,f,i). Associated F 1s spectra shown in Figure S2 (Supporting Information). Composition % values shown in Table S2 (Supporting Information).

The F 1s signal in the wide scan remains high (at 38.9%), again indicating the coating is thinner than the XPS sampling depth.

In the XPS C 1s core line spectrum (Figure 3h) a strong signal from the CF_2 group remains, alongside the new signal introduced by the HPG at 286.5 eV indicative of the C—O—C moiety, accounting for 35.0% of the C 1s signal. The presence of the CF_2 (and other CF_n and OCF_n signals) indicates a thin HPG coating less than the XPS sampling depth (<10 nm). Again, we would expect the true C—O content of the coating to be higher than this indicates, with a substantial portion of the C 1s signal arising from the substrate. The O 1s signal (Figure 3i) shows the dominant C—O—C character (75.6%) centered at 532.6 eV, indicating HPG formation, alongside O═C, C—OH, and O—C—F_n binding environments which come from the coating and underlying PTFE.

To further compare the consistency of HPG coatings, HPG was grafted onto Si and Al (Figures S3 and S4, respectively, Supporting Information). These samples also display a characteristic C—O peak in the C 1s spectra, accounting for 83.8% and 79.3% of the C 1s signal for Si and Al, respectively, and indicate a thin coating with substrate signals clearly detectable in the wide scan spectra (Table S3, Supporting Information).

To further elucidate the likely structure of the HPG coating, end group labeling was performed by derivatization with trifluoroacetic anhydride (TFAA) on HPG coated TiSi substrates. The derivatization mechanism is shown Figure S5 (Supporting Information). Likely end groups that terminate the HPG coating, C—OH, C═O, and COOH, are all known to react with TFAA to form —O—C(═O)—CF_3.[67] By using XPS to measure fluorine concentration in the wide scan spectrum or CF_3 percentage composition in the C 1s core line spectrum (Figure S6, Supporting Information), we can estimate the proportion of end groups in the HPG coating using the following formula[68]

$$[X] = \frac{[CF_3]}{100 - 2 \times [CF_3]} \cdot 100\% \quad (1)$$

where [*X*] represents the labelable end group concentration, and [CF_3] is the fraction of CF_3 carbon in the C 1s spectrum groups.[68,69] While the derivatization introduces HC contamination, which is not uncommon, from the CF_3 and CO peak compositions in the C 1s spectrum, and the introduction of a correction factor for HC contamination (by comparing the C—O/C—R ratios of the spectra before and after TFAA labeling), we are able to calculate that 5.5%–6% of carbons are end groups. It follows that for every end group there are ≈16–18 C—O—C repeats and from protein adsorption data (Section 2.2.1), we speculate that HPG chains are likely to pack in a regular and tight fashion across the substrate surface.

In addition to XPS measurements, HPG coatings were studied using contact angle measurements and atomic force microscopy (AFM). Contact angle measurements made on Si, TiSi, and PTFE (Table S4, Supporting Information) all show a reduction in water contact angle between uncoated and coated samples, further indicating that similar coatings have been formed on each substrate.

AFM was used to confirm the uniformity and pinhole free nature of the HPG coatings on TiSi and Si, and to estimate the thickness of the coating. After grafting of HPG onto TiSi, the morphological feature of the plasma activated substrate were not visible (Figure S7, Supporting Information), indicating HPG forms a uniform and pinhole free layer across the surface. Interestingly, part of the HPG formed large agglomerates. Scratch tests were performed which produce a line profile to indicate sample thickness. Typically, the line profile should display a step, the height of which can be measured to provide an approximate sample thickness. From the representative scratch test performed on HPG grafted onto TiSi the coating thickness is as low as 1.27 nm. However, we note that the RMS roughness of the coating inside the scratched area (4.38 nm) is higher than the plasma activated surface, suggesting the presence of a strongly bound HPG layer that could not be removed. We therefore note that this value is a lower bound for coating thickness. Analogously, the HPG coating on Si is found to be uniform and pinhole free with a thickness as low as 0.31 nm thick (again, as a lower bound). The thinness of these films is corroborated by the clear visibility of substrate signals in the XPS data.

2.2. HPG Resistance against Protein Adhesion and Biofilm Formation

2.2.1. Protein Adsorption

HPG coatings on TiSi (and ethanol (EtOH) plasma polymers, 80 nm thick, used as a control experiment) were exposed to single solutions of albumin (the most abundant blood protein)[70] and fibrinogen (an adhesive protein, implicated in cell binding),[71] using an adapted protocol from Wu et al.[72] After incubating for 1 h, samples were washed three times in phosphate buffered saline (PBS) to remove loosely bound (termed "reversibly adsorbed") proteins. With further samples, after protein adsorption, washing was repeated with a more rigorous protocol using sodium dodecyl sulphate (SDS) solution. Any remaining protein was deemed to have irreversibly attached ("retained protein").[73]

XPS was used to detected protein using the unique N 1s signal. Figure S8 (Supporting Information) demonstrates that of the materials tested, the HPG coating exhibits the highest degree of resistance to initial (reversible) protein adsorption (the N 1s signal accounted for 1.4% and 4.5% of the atomic composition when exposed to albumin and fibrinogen, respectively), and it is the only coated sample tested where retained protein adsorption was beyond XPS detectability (uncoated Si and uncoated PTFE also showed no detectable retained protein adsorption). Previous studies have shown that nitrogen content of around 1% corresponds to 10–25 ng cm^{-2} of fibrinogen at the surface (though this is substrate dependent and may also depend on the organization of the adsorbed protein layer).[74] The level at which protein adsorption becomes detrimental for platelet attachment and activation is believed to be c. 30 ng cm^{-2}.[75,76]

This result is consistent with earlier work, where a much thicker HPG coating of 25 nm effectively resisted reversible protein binding and is termed "low fouling", based on a low level of protein detected by XPS (< 1%N) and secondary ion mass spectrometry.[32] Our study further exemplifies the remarkable quality of HPG which does not permit irreversible attachment of proteins, unlike other coated materials, which lends to the hypothesis that HPG could be excellent for both hemocompatibility and nonbiofouling applications. In the case of reversibly bound protein, an interesting question is whether this protein is held at the HPG surface, or whether it might conceivably have penetrated within the coating. To investigate these possibilities, XPS ion milling was employed to etch the reversibly bound protein and HPG coating.

XPS ion milling, using a gas cluster ion source (GCIS), allows depth profiling of organic materials, removing polymer layers with minimal damage to the underlying polymer structure.[77] Prior to protein depth penetration measurements, GCIS milling settings were tested on HPG on TiSi coatings, milling from the air-interface, through the coating to the substrate-interface. Reaching the substrate is evidenced by significant removal of carbon (Figure S9 (Supporting Information) shows wide scan spectra before and after etching). The core line spectra for C 1s, O 1s, and TiSi 2p were collected at 10 s etch steps, over a 1000 s total etch time. **Figure** 4a–d shows the evolution of the C 1s spectra as the HPG coating is removed, with the initially dominant C—O environment gradually reducing over time. Plotting the atomic composition (Figure 4e) shows that by 350–400 s etch time, the Ti 2p, O 1s, and C 1s signal plateau, indicating that the substrate has been reached. Within the C 1s spectra, the removal of HPG coating was defined as the time at which the C—O component area (CPS eV) plateaued (Figure 4f). For HPG on TiSi substrate this occurred at around 350 s. After this point the C 1s, O 1s, and Ti 2p composition remained unchanged, suggesting that the GCIS is only able to remove HPG and does not remove the underlying substrate.

After establishing suitability of ion milling for depth profiling HPG coatings, HPG on TiSi was exposed to albumin, washed with PBS and then milled (initial and final wide scan data presented in Figure S10, Supporting Information). For each 10 s etch C 1s, O 1s, Ti 2p, and N 1s core line spectra were collected (**Figure 5**). The N 1s signal was observed to rapidly change over the first 0–100 s of etching. The dominant N—C peak reduces by over 50%, signifying the rapid removal of the protein. Figure 5a–f shows the evolution of the C 1s and N 1s spectra during the ion mill. Figure 5g shows the atomic composition against etch time,

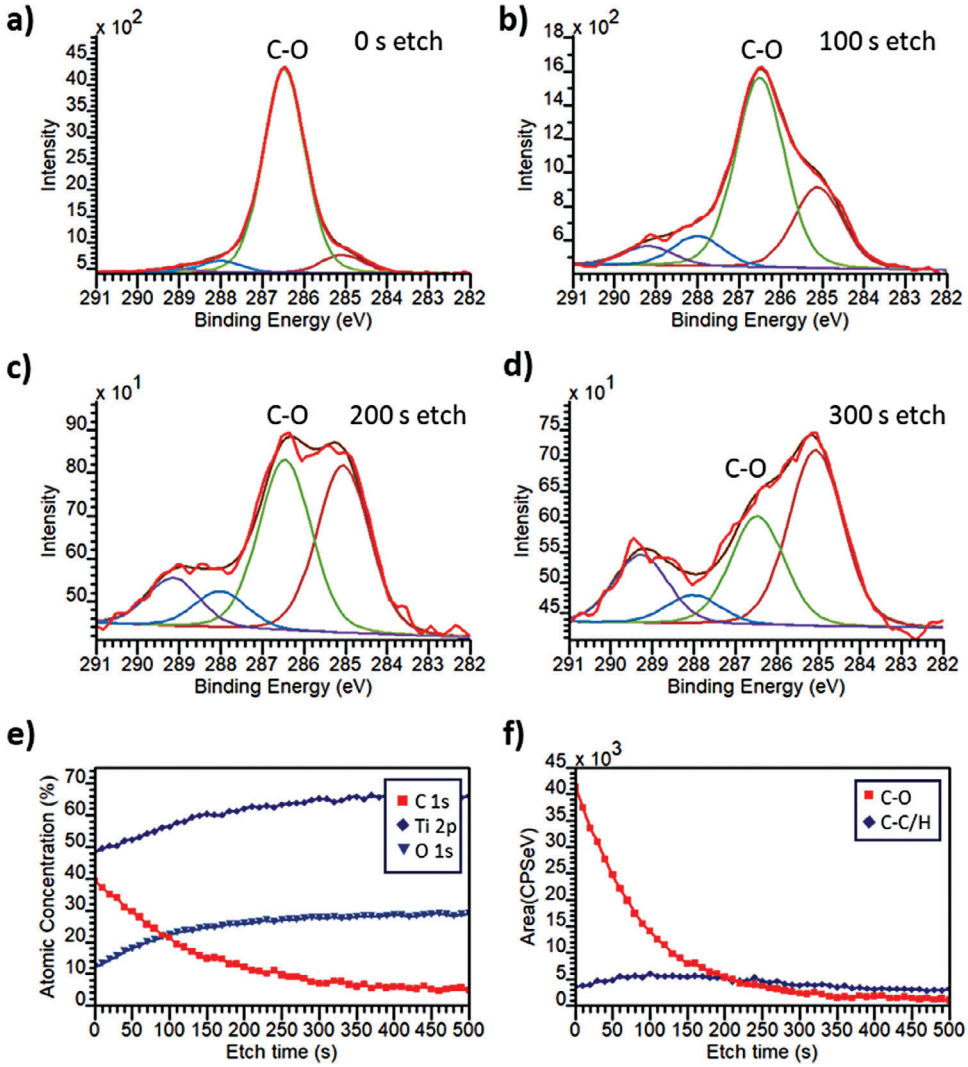

Figure 4. Ion milling of HPG coating on TiSi substrate. a–d) C 1s core line spectra at a) 0 s milling, b) 100 s milling, c) 200 s milling, and d) 300 s milling. e) Atomic composition (%) plotted against etch time (s). f) C 1s C—C/H and C—O component area plotted against etch time. C—O area plateaus by 350 s, indicating removal of the C—O based HPG coating. Smoothing applied to all ion mill spectra (Savitzky–Golay, quadratic, width 7). Corresponding wide scan spectra available in Figure S9 (Supporting Information).

showing a clear reduction in C 1s and N 1s and corresponding increase in Ti 2p and O 1s as both the protein and coating are etched away through to the substrate.

As shown in Figure 5a–f,h, the etch rate of N—C (amide) and C—O (HPG) are different, with the N—C plateauing to a minimum value by 100–150 s, and the C—O continuing to reduce until 350–400 s etch time (similar to HPG without albumin in Figure 4). While three distinct peaks can still be observed in the N 1s spectra (Figure 5f), these are associated with the substrate, and can also be identified at the HPG/substrate interface in HPG on TiSi that has not been exposed to albumin (Figure S9c, Supporting Information). A credible explanation that fits all these data is that the HPG coating "holds" proteins at its surface, preventing protein molecules from moving within the coating to the TiSi interface. To strengthen this argument a control experiment was carried out by depth profiling in an 80 nm EtOH PP coating, following exposure to albumin (Figure S11, Supporting Information). Within this sample, protein (from N1s signal at 400.19 eV) etches at the same rate as EtOH (from C1s C—O signal at 286.39 eV), and, while the substrate is still not reached after 1500 s etching due to the coating thickness, the continued presence of N—C throughout the mill indicates that some protein has migrated within the coating rather than being held at the coating surface.

2.2.2. Microbial Colonization and Biofilm Formation

The ability of HPG coatings to prevent bacterial colonization and biofilm formation, in two Gram-positive and three Gram-negative species, were tested independently in two laboratories at the Centre for Cancer Biology, University of South Australia (UniSA, Australia) and at the Royal Lancaster Infirmary (RLI, UK). At UniSA, uncoated and HPG coated TiSi substrate was

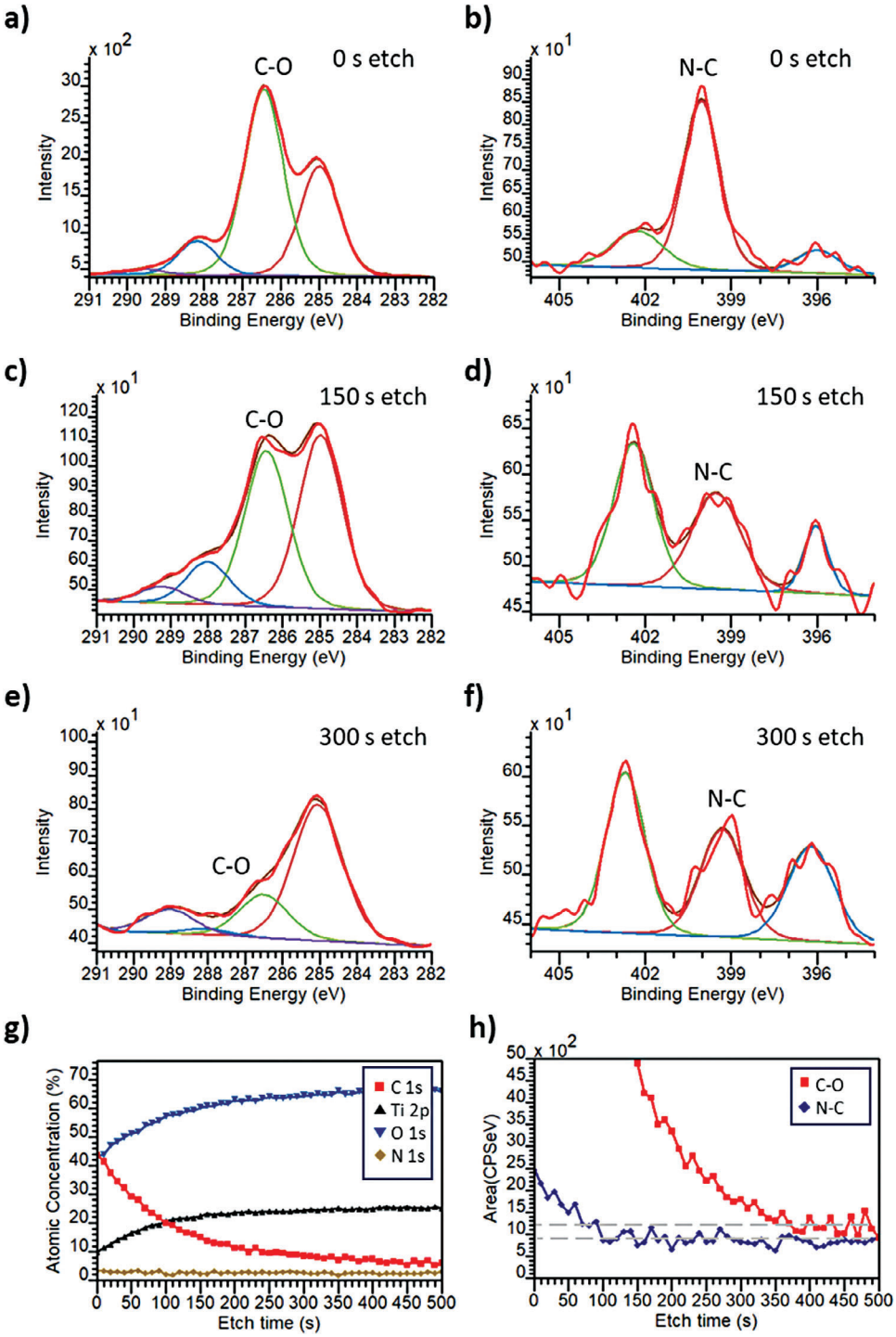

Figure 5. Ion milling of HPG coating on TiSi substrate exposed to albumin. a–f) show C 1s and N 1s spectra at points throughout the milling process: a) C1s and b) N 1s at 0 s mill time. c) C 1s and d) N 1s at 150 s mill time. e) C 1s and f) N 1s at 300 s etch time. g) Atomic composition (%) plotted against etch time (s). h) C 1s C—O and N 1s N—C component area plotted against etch time, showing the time at which N—C plateaus, indicating removal of protein, is between 100 and 150 s. C—O area plateaus by 350 s, indicating removal of the C—O based HPG coating, indicating that protein is held at or near the coating surface. Smoothing applied to all ion mill spectra (Savitzky–Golay, quadratic, width 7). Corresponding wide scan spectra available in Figures S9 and S10 (Supporting Information). Positive control data (EtOH plasma coating) provided in Figure S11 (Supporting Information).

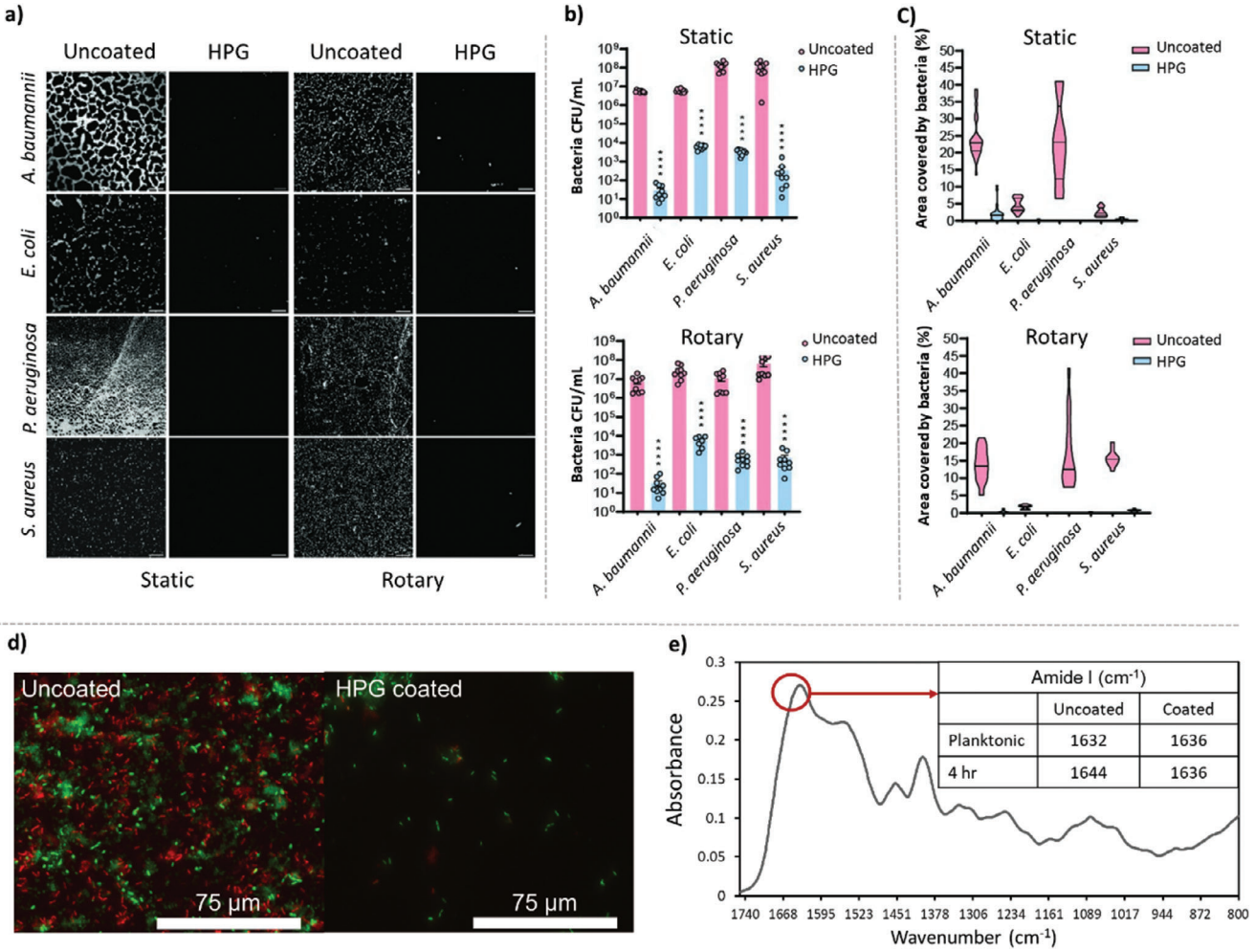

Figure 6. Characterization of uncoated and HPG coated Ti a–c) or Al d,e) substrates following with 5 bacterial species (*E. coli*, *S. aureus*, *P. aeruginosa*, *A. baumannii*, *S. epidermidis*). a) Representative bright-field microscopy images of crystal violet stained HPG and uncoated samples, after 24 h static and rotary incubation with each strain. Area of surfaces exposed to bacteria were identical with a surface-area-to-volume ratio of 0.227. b) Summative graphs displaying the number of bacteria adhering to the surface of each HPG coated (blue) and uncoated (pink) sample, after 24 h static and rotary incubation with each strain. Bars represent the mean with dots of individual experiments, ****$p < 0.0001$, Student's *t*-test. c) Summative graphs quantifying the total area coverage (%) per sample, after 24 h static and rotary incubation with each strain. d) Fluorescence microscopy live dead stain demonstrated exceptionally low colonization of HPG coated glass. e) FTIR spectroscopic analysis reveals unshifted amide I protein region on HPG coated aluminum, suggesting the phenotype of the bacteria has not switched from planktonic to biofilm. Further evidence given in Figure S4 and Table S5 (Supporting Information).

examined for the extent of colonization after 24 h of exposure to cultures of *E. coli*, *S. aureus*, *P. aeruginosa*, and *A. baumannii*, using standard microbiological methods (see the Experimental Section). The CFU reflect the number of viable bacteria adhered on to the surface of the wafers and crystal violet staining reflects the biofilm and any other bacterial debris. **Figure** 6a–c provides evidence of significantly lower bacterial attachment visibly observed on the HPG coated surfaces ($p < 0.0001$), compared to the uncoated surface. Furthermore, the number of live bacteria adhering to the HPG was quantified, and was consistently reduced compared to the uncoated control, across all species. Most promisingly, the colonization of *A. baumannii* was extremely low under static and rotary conditions evidenced by both % area of bacterial coverage and the number of bacteria adhering to the surface, which remains below 10^2 CFU mL^{-1}. This result is particularly significant because *A. baumannii* is extremely prevalent in hospital acquired infections originating from the use of a wide range of medical devices.[78]

At the RLI, HPG coatings were tested against a rapid biofilm forming strain of *S. epidermidis*. Figure 6d shows fluorescence microscopy live dead staining of *S. epidermidis*, demonstrating exceptionally low colonization of HPG coated glass. While standard microbiological characterization can demonstrate low bacterial attachment, they are unable to define the biofilm phenotype.[79] A novel FTIR spectroscopy technique was used to determine whether attached microorganisms were in the planktonic or biofilm state.[80] Figure 6e shows the result from this FTIR analysis of uncoated and HPG coated aluminum after 4 h bacterial exposure. Aluminum substrates were used due to the incompatibility of Si substrates with FTIR (evidence of HPG coatings on Al is

shown in Figure S4, Supporting Information). FTIR allowed evaluation of the protein composition of a sample, which can be used to monitor the phenotypic switch from planktonic to biofilm. For *S. epidermidis*, the centroid of key protein region (amide I) appears at 1634 (± 2) cm^{-1} (when analyzed on aluminum foil substrates) for planktonic samples. The amide I peak is markedly shifted in biofilm samples to 1644 cm^{-1}, signifying a chemical change coincident with the phenotypic switch to an adherent cell population.[80] On 4 h incubation, a peak shift to 1644 cm^{-1} was recorded for uncoated samples. In contrast, on the HPG coated sample, no shift in the protein peak position was observed, indicating that even where bacterial colonization has occurred, a biofilm has not formed.

Overall, there is a consistency in results from both institutions revealing a markedly reduced level of bacterial colonization on HPG coated surfaces, and longer-term ability of HPG to prevent biofilm formation on the surface when examined with single species models.

2.3. HPG Interaction on Blood Contact

To study HPG – blood interactions, HPG coatings were applied to nitinol and SS sheets and stents (as shown in Figure 1). The coatings obtained were identical to those discussed earlier.

2.3.1. Platelet Adhesion and Activation

For blood-contacting materials, platelet binding and activation is one of the first defenses in the foreign-body-response, ultimately leading to thrombosis.[7] We began testing the hemocompatibility of HPG-grafted materials by investigating the interaction with freshly isolated human platelets.

In line with our previous work,[32] HPG was grafted onto PS that had been spin-coated onto a silicon wafer to allow for easy chemical (see XPS analysis in Table S5 and Figure S12, Supporting Information) and biological analysis of the flat and pure substrate. Isolated platelet suspensions from human volunteers were incubated on the surfaces for 1 h, washed and stained. Platelets were found to bind in abundance to the plasma-activated PS controls, as seen in **Figure** 7a. This was not unexpected as these surfaces are analogous to tissue culture PS and highly susceptible to cell attachment. Conversely, the HPG-grafted PS was found to be extremely resistant to platelet binding, which was reduced by >99.99%, with respect to the PS control ($p < 0.0001$) (Figure 7a,b).

Multiple morphologies were observed for the bound platelets that ranged from small and rounded through to large and spread with pseudopodia. For analysis, the platelets were categorized into three distinct subpopulations and partitioned by visual assessment from the fluorescent micrographs, as summarized in Figure 7b. These morphologies are a reliable indicator of the state of activation of the platelets, with greater cell spreading associated with greater activation.[81,82] Small rounded platelets are considered to be in a nonactivated resting state.[83] The PS controls consisted of ≈84% of platelets that were completely spread, ≈6% that were starting to spread (dendritic morphology) and ≈10% that remained round. It is our contention that a vast majority of the platelets bound to the PS were activated and would be

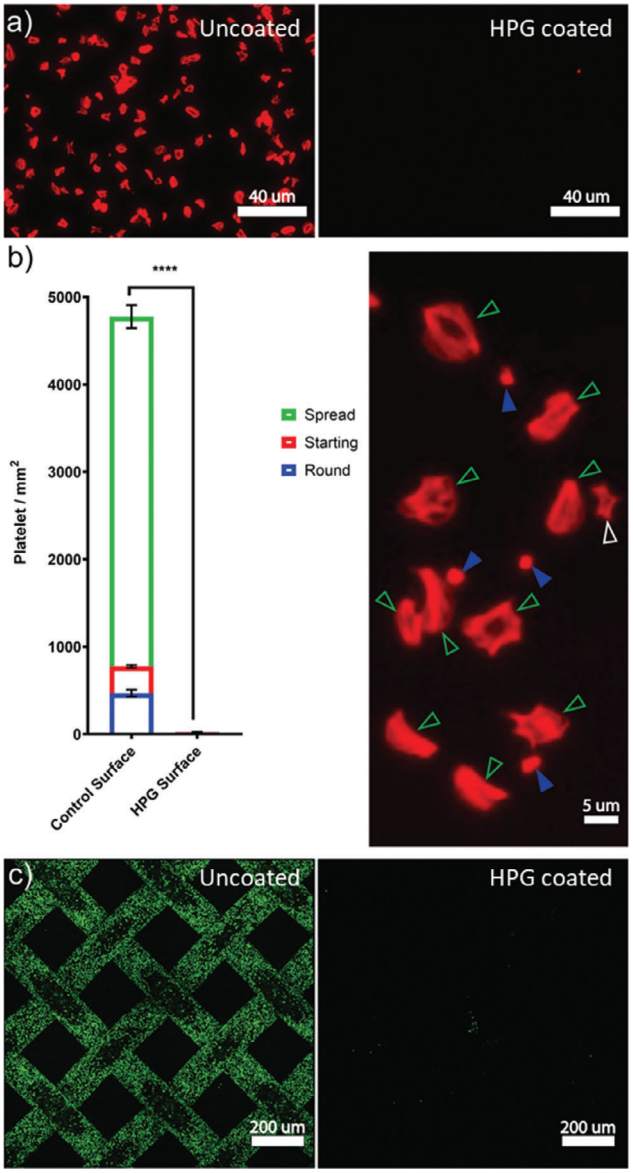

Figure 7. Platelet binding. a) Platelets isolated from human blood bind to plasma-treated PS but not HPG-coated surfaces. b) Quantification of platelets (spread in green, starting in red, and round in blue) bound to PS and HPG surfaces. Data represent mean ± SEM,**** = $p \leq 0.0001$ unpaired Student's *t*-test. Examples of spread (green hollow arrowheads), starting to spread (white hollow arrowheads), and round (blue solid arrowheads) morphologies. c) Human platelets bind to a SS mesh (left) but not to HPG-coated SS mesh.

contributing to thrombus formation in a whole-blood system.[84] There were no spread platelets found on the HPG-coated samples. These data suggest that the HPG coating almost completely prevented platelet attachment and activation in this isolated system.

Flat substrates are often necessary to validate the performance of a medical coating, but they do not present the technically challenging aspects associated with 3D and multifaceted devices, such as stents. Moving toward a more geometrically complex model system, SS mesh, with 90 µm thick woven wires, was

chosen to represent a more stent like architecture. HPG modification of SS mesh followed the same process as for flat PS and yielded the characteristic etheric carbon peak expected for a suitable HPG coating (Table S5 and Figure S12, Supporting Information). Following incubation with isolated platelets, washing and staining, the control SS mesh was clearly visualized by fluorescence microscopy due to the abundance of bound platelets (Figure 7c). Once again, it was not unexpected that large quantities of platelets would bind to the uncoated control samples since this is a known limitation of clinical-grade SS stents.[85] On the other hand, the HPG-grafted SS mesh exhibited very few platelets (99.8% reduction over control, calculated by fluorescent area over equivalent fields of view), despite the increased complex geometry and potential places for the platelets to lodge. Notably, the few bound platelets on the HPG-coated SS mesh were not associated with any particular feature of the woven mesh, such as the cross-over joints, as might have been expected. Achieving this very low binding of platelets on a substrate with much greater geometric complexity and on a material of clinical relevance demonstrates the robustness and potential of the HPG coating to provide benefits to existing endovascular devices. The result also confirms the uniformity of our HPG coating process, able to protect the more hidden surfaces at the cross-over joints.

2.3.2. HPG Prevention of Stent Thrombosis Ex Vivo

Building on the reduced platelet binding on SS mesh, the HPG coating was further challenged on clinical-grade nitinol stents using whole blood under conditions of shear flow (**Figure 8**). Here, we investigated ST in HPG-grafted nitinol stents exposed to fresh human blood, using a modified Chandler loop assay.[86,87] For these studies, commercially available 6 mm diameter stents were cut into sections consisting of 4 struts and coated with HPG following the same process as previous substrates. Successful HPG grafting was again confirmed by a characteristic etheric carbon peak in the high resolution XPS spectra (Table S5 and Figure S12, Supporting Information).

A typical Chandler loop assay consisted of one bare (control) stent section and up to four HPG-grafted stent sections inserted into separate loops, which were then filled with fresh human blood. Simulated blood flow was maintained in each loop at ≈5 dyn cm^{-2} at 37 °C for 2 h. A representation of the outcome of these assays is presented in Figure 8b and shows a significant difference in performance between bare nitinol and HPG-grafted nitinol stent sections. Every bare nitinol control was completely occluded by the completion of the assay, however, clots varied in size and weight between donors. In stark contrast, the HPG-grafted stent sections consistently appeared free from any clot formation and weighed significantly less than the controls (Figure 8c).

To interrogate further and identify any cellular interactions that might be occurring at the surface, scanning electron microscopy (SEM) images of the stent samples were analyzed. As expected, the control stents were completely covered in large networks of fibrin strands containing trapped erythrocytes, which were absent from HPG-grafted stent sections (Figure 8d). This was consistent with the reduced platelet binding on HPG-coated surfaces and supports the hypothesis that the prevention of

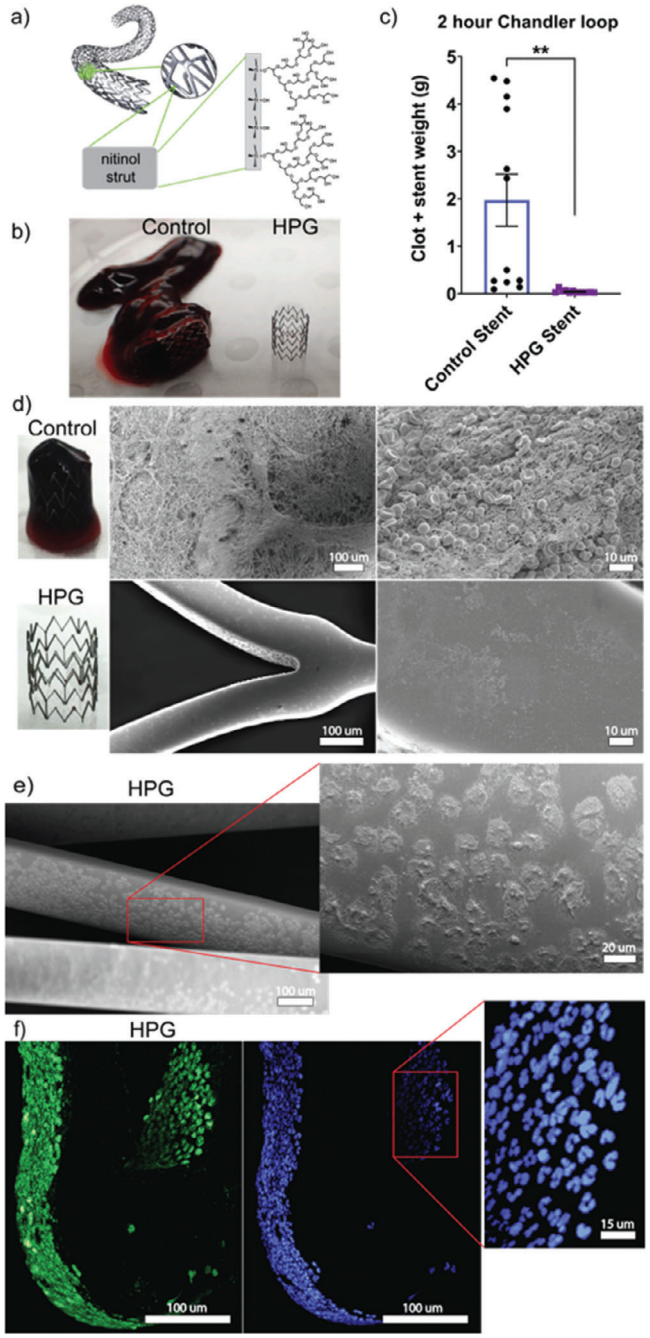

Figure 8. HPG-coated stents prevent platelet binding. a) Schematic of a stent made from nitinol struts coated with HPG. b) HPG coating prevents blood from clotting in a Chandler loop. c) Comparison of combined weight of clot and stent of a control stent versus an HPG-coated stent after 2 h in a Chandler loop. Data represent mean ± SEM, $n = 12$ independent experiments, ** = $p \leq 0.01$, Student's t-test. d) Magnified images of control and HPG stent, and electron microscope images of platelets and fibrin networks bound to them. e) Cells predominantly bind to strut areas that are perpendicular to the blood flow. f) Fluorescence microscopy images of lobulated mononuclear cells consistent with neutrophils bound to HPG-coated stent struts. Cells were stained with CFDA SE Cell Tracer in green and DAPI in blue.

platelet binding reduces thrombosis on HPG-grafted stents. The SEM micrographs did however uncover the presence of a population of cells lining, almost exclusively, the area of the stent struts that lay perpendicular to the direction of blood flow (Figure 8e). These areas are known to create eddies in the flowing blood and potentially cause the blood to stagnate at these locations.[88] While platelets and erythrocytes could be ruled out due to the size and shape of the cells, SEM analysis does not allow the nature of these cells to be determined. However, fluorescence microscopy revealed the population consisted of lobulated mononuclear cells (Figure 8f), consistent with neutrophils. Furthermore, our previous studies have determined that neutrophils are a select population of blood cells that can bind to HPG under static conditions.[32] This likely reflects the difference in binding between high and low shear force for these cells.

Further analysis of the HPG coating was designed to establish suitable robustness and stability to survive packaging, sterilization, and long-term storage at ambient conditions (Figures S13–S20, Supporting Information). Packaging for nitinol stents involves high mechanical forces to first compress the stent, then slide it into the polymer sheath that keeps it compressed until deployment. The long-term stability of HPG-grafted nitinol stent sections was assessed over a 12-month period using the Chandler loop assay to test stored samples every 3 months (Figure S17, Supporting Information). Preliminary results indicated that the HPG coating on stents retained its ability to prevent thrombosis for up to 12 months, when stored under ambient conditions. In a further study, full-length clinical grade stents (6 mm × 40 mm) were HPG-grafted, packaged, ethylene oxide-sterilized, and stored under ambient conditions. Once again, stability of the coating was tested every 3 months for up to 12 months (Figure S18, Supporting Information) and again at 44 months (Figure S20, Supporting Information). The Chandler loop assay results in this repeat study confirm that the HPG coating is robust and able to retain its antithrombogenic properties throughout the packaging and sterilization process and remained stable at room temperature for up to 44 months. Similar results were observed for much larger diameter HPG-grafted venous stents (14 mm × 60 mm) which were also packaged and sterilized (Figure S20, Supporting Information).

Following on from this encouraging demonstration of the HPG coating providing significant benefits to blood-contacting devices by reducing their thrombogenic potential, further investigations were necessary to determine if the HPG coating elicited any downstream effects, through activation of other pathways, above the level commonly seen for current implants.

2.3.3. Complement and Neutrophils are not Activated by HPG

The activation of complement and neutrophils on HPG-grafted stents was investigated using the Chandler loop assay followed by testing of the blood from the loops, using an accredited commercial pathology testing laboratory. For these experiments, blood was collected in lithium heparin Vacuette tubes to delay clotting during testing. HPG-grafted stents were compared to uncoated nitinol stents. Two additional control samples were analyzed: blood that was added to a loop without any device present; and blood that had not been exposed to the Chandler loop assay. The experiment was repeated with blood from five healthy donors. Results, summarized in **Figure 9**a, indicated no detectable loss of complement components for any of the tested samples. Complement component levels remained consistent across the samples within each experiment with only small variations seen between donors, with respect to the reference serum composed of pooled human samples. This analytical technique is highly sensitive to the loss of complement components that would indicate activation of the complement pathway. It was evident from these results that neither the uncoated control stents nor the HPG-grafted stents had activated the complement pathway, corroborating previous findings.[49] Furthermore, there was no significant difference between the samples with respect to reactive oxygen species (ROS) detection (measured by the dihydrorhodamine-123 oxidative burst assay), which is an indicator of neutrophil activation (Figure 9b). All tested samples remained two orders of magnitude lower than the artificially activated sample that represented a serious clinical event. Therefore, it was concluded that neutrophils were not activated through transient contact with either the control or HPG-grafted stents under flow.

2.3.4. HPG-Grafted Materials do not Elicit Inflammatory Responses In Vivo

To explore potential adverse immune reactions triggered by the HPG coating once implanted into tissue, a preclinical rodent toxicity study was undertaken. HPG-grafted and bare nitinol disks implanted subcutaneously under the back skin of mice, for 1 or 5 weeks, were used to investigate potential acute and chronic inflammation, respectively. Histology on the explanted back skin that sat directly above the implanted disks indicated there was no significant alterations to overall thickness between the control disk, HPG-grafted disks, and nontreated normal back skin after 1 or 5 weeks (**Figure 10**b). When each of the four layers, epidermis, stroma, muscle, and fat were measured separately (Figure 10d,e), both the control disks and the HPG-grafted disks at 1 week showed a statistically significant increase in fat layer thickness, with respect to untreated back skin. However, there was no difference between fat layers of the control disks and the HPG-grafted disks. Furthermore, at 5 weeks the skin from the HPG-grafted disks had a significantly thinner fat layer than the normal untreated skin, while the uncoated control disk had returned to the same thickness as the normal untreated skin. While it was not expected that the bare nitinol disks would illicit an inflammatory response, this analysis confirms that the addition of an HPG coating does not induce an acute or chronic inflammatory reaction.

2.3.5. HPG-Grafted Stents Reduce Restenosis in ApoE$^{-/-}$ Mice

Finally, we tested the effect of the HPG-coating on ISR using an in vivo model. We used the carotid inter-position grafting model in ApoE$^{-/-}$ mice in which a stent is deployed into a donor descending thoracic aorta before grafting into the carotid artery of a recipient mouse (**Figure 11**a).[89] The study compared HPG-coated SS stents with bare SS stents over a period of 28 days. Analysis of the explanted stents, following fixation and sectioning, indicated that

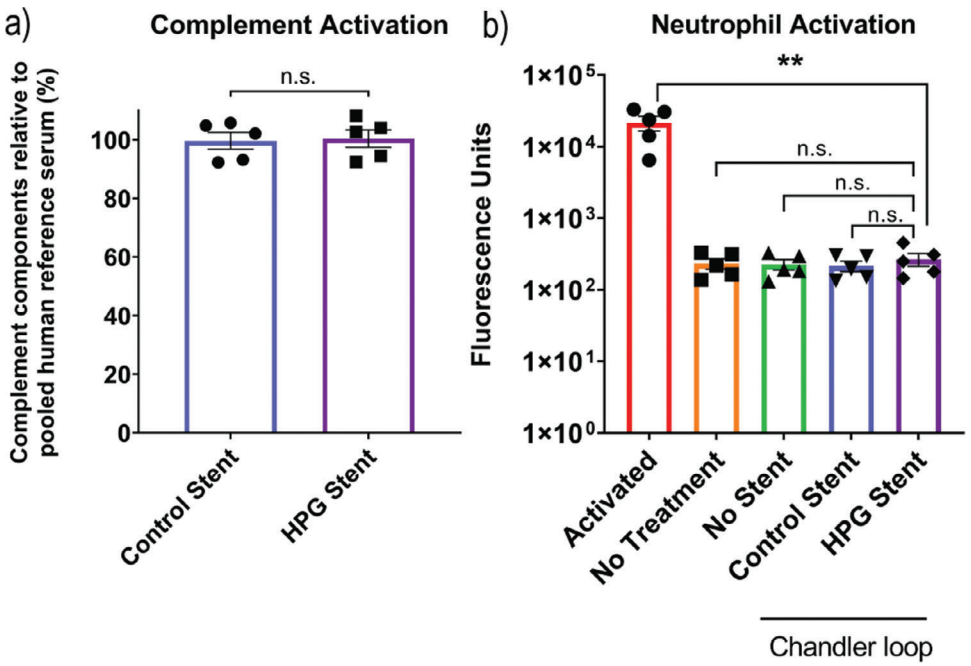

Figure 9. HPG-coated stents do not show any loss of compliment components nor trigger neutrophil activation. a) There is no significant difference between the control stent and HPG stent compared to the pooled human reference serum. b) The detected (ROS) are significantly lower in the controls and HPG stent than the activated control. Data represent mean ± SEM, $n = 5$ independent donors, ** = $p \leq 0.01$, unpaired Student's *t*-test. n.s. not significant.

all control stents had become completely occluded (restenosed), largely by proliferating vascular smooth muscle cells, with resulting neointimal formation (Figure 11b). In stark contrast, HPG-coated stents had a large, fully patent lumen with minimal neointimal hyperplasia (Figure 11e). Neointima thickness measurements were taken to the center of the occluded control stents (500 µm) and found to be completely occluded along the entire length of 5 out of the 8 control stents. The average area of restenosis for the control stents was 0.84 mm^2. The HPG-coated stents averaged a neointima thickness of 209 µm (measured from behind the stent strut to the edge of the new lumen), giving an average restenosis area of 0.55 mm^2 and, except 2 out of 8 HPG-coated stents that completely occluded, remained patent along the entire length, resulting in a significant reduction in restenosis over the bare control stents. Area of restenosis in HPG samples was measured by tracing the highly conserved tunica media (Figure 11f,g) and subtracting the area of the new lumen (Figure S21, Supporting Information). Area of restenosis for controls was measured from behind the stent struts but the original vessel wall had to be estimated due to severe degradation of the tunica media in all samples (Figure 11d,e).

3. Discussion

HPG-grafted substrates have already demonstrated very effective resistance to surface adhesion of a range of proteins and cells by these authors and others.[33,34,45,53,54,59] Furthermore, the biocompatibility and hemocompatibility of HPG in solution have been previously documented, with in vitro and in vivo assays indicating HPG has no adverse effects on complement activation and platelet activation.[49,90–92] Despite the promising evidence for clinical application, the biocompatibility, hemocompatibility, and durability of HPG on vascular devices, have not been extensively tested. This has been in part due to the considerable limitations with previous methods of achieving a commercially viable HPG coating on materials, which were complex, costly, and involved the use of hazardous chemicals.[33,56,60,93,94] We sought to overcome these limitations with a novel coating process that is simple, environmentally friendly and commercially viable.

Our HPG coating process involves plasma activation of the substrate prior to immersion in glycidol. While we have previously demonstrated this process on polystyrene on Si,[32] here we demonstrate that the process can be applied to a wide range of substrates, including Si, Ti, Al, steel, nitinol, PTFE, and PS, and can be applied to both 2D substrates and 3D stents. XPS analysis of substrates before and after plasma activation shows an increase in oxygen content and the formation of an oxygen rich surface, featuring highly reactive sites that facilitate the glycidol grafting process. The subsequently formed HPG coating is characterized by a strong etheric (C—O—C) component, typically accounting for 65%–85% of the C 1s signal. End group labeling with TFAA suggests that the coating is primarily formed of etheric chains, with c. 6% of carbons as end groups. XPS and AFM analysis of HPG coated show that the coating formed is ultrathin (a few nm thick), conformal and pinhole free.

Adhesion of proteins to surfaces is a key step in foreign body response, cell attachment and biofouling processes. Minimizing protein absorption is therefore a major goal of low/nonfouling coatings. Our data indicate that in addition to reduced protein adsorption, the reversibly bound protein is held at the coating surface, rather than migrating throughout the coating and

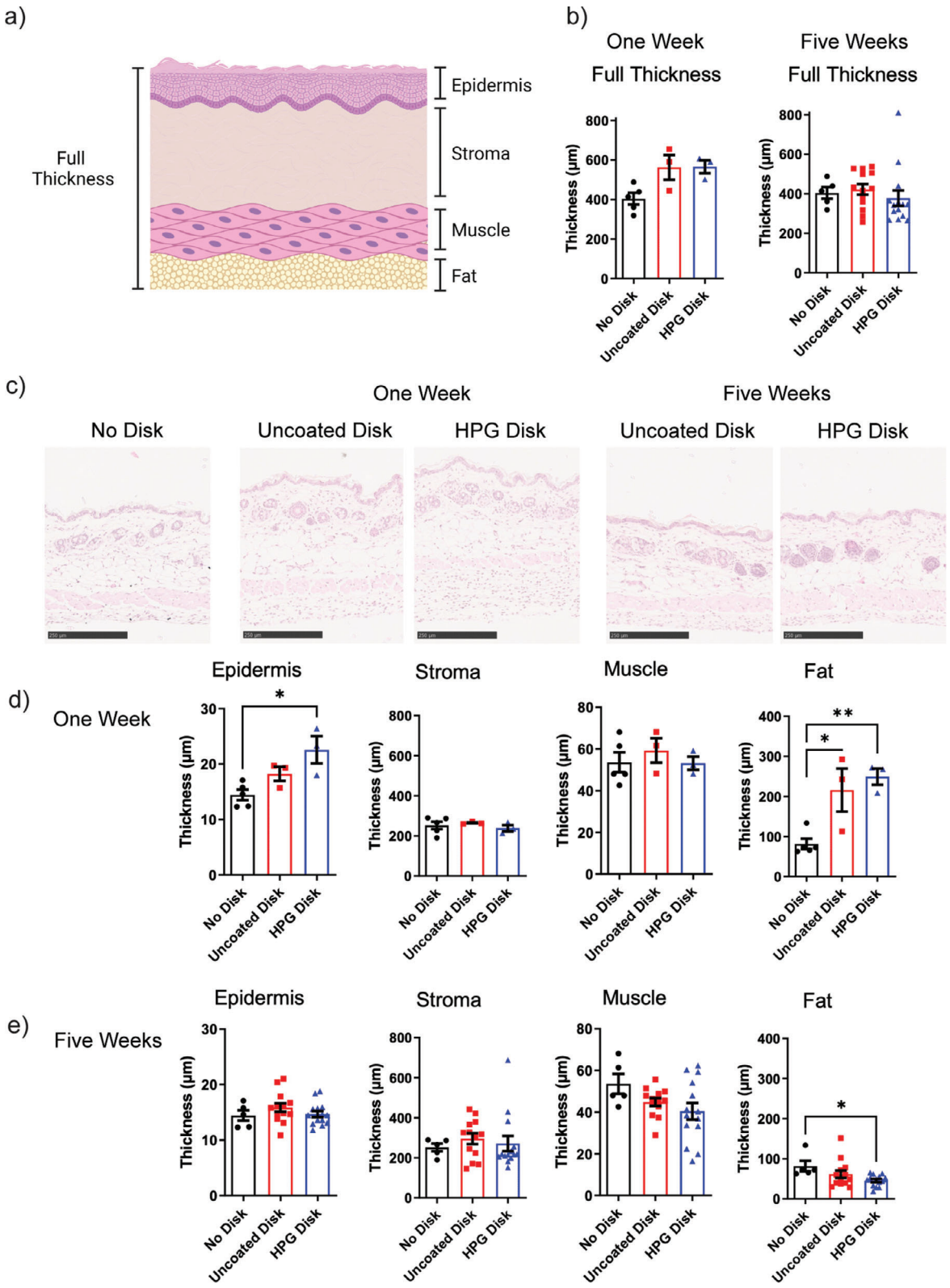

Figure 10. HPG coating does not elicit an inflammatory response in vivo. a) Schematic of cross section through murine back skin. b) Analyzed full skin thickness following 1 and 5-week time points with uncoated (red) and HPG-coated nitinol disks (blue) compared to back skin of mice which received no disk (black). Data represent mean ± SEM, $n = 3$–15 mice, * = $p \leq 0.05$, ** = $p \leq 0.01$ unpaired Student's *t*-test. c) Representative images of sections stained with H&E after 1 and 5 weeks. Scale bars indicate 250 µm. d,e) Analyzed thickness for each individual skin layer for 1 and 5 weeks, respectively. Data represent mean ± SEM, $n = 3$–15 mice, * = $p \leq 0.05$, ** = $p \leq 0.01$ one-way ANOVA.

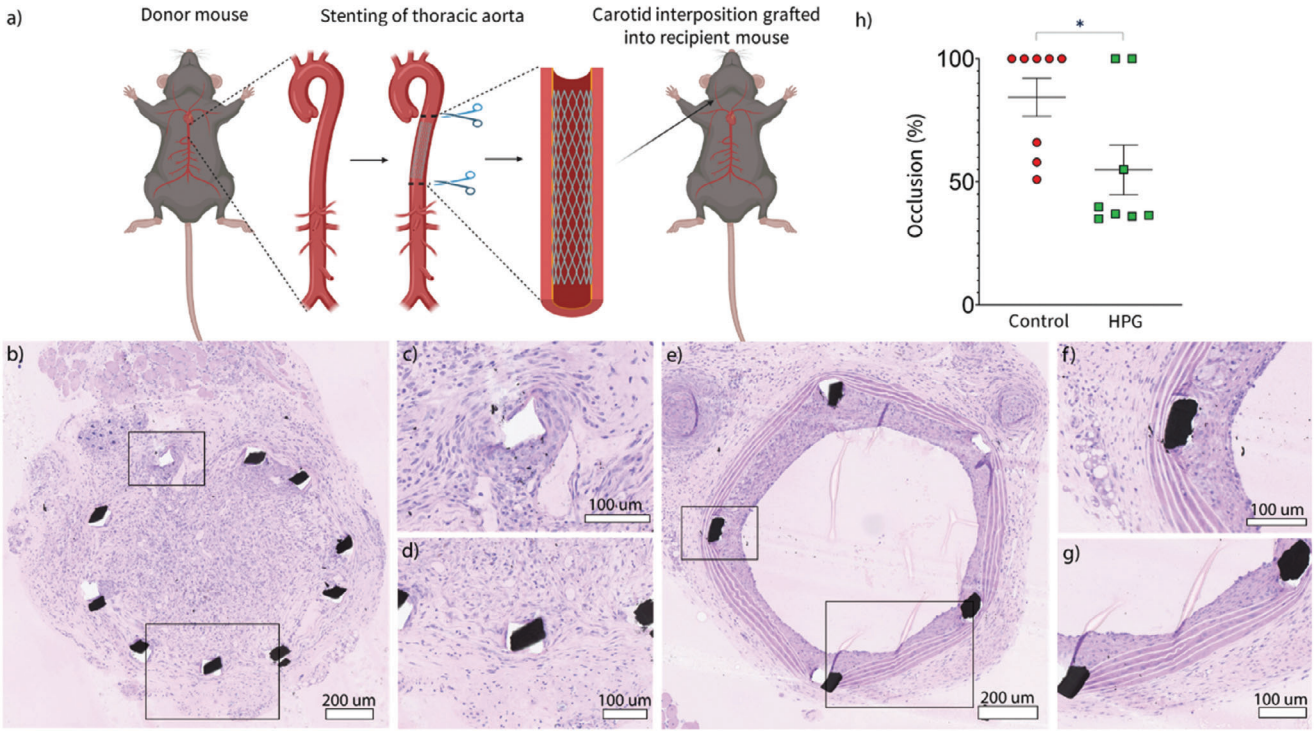

Figure 11. HPG-grafted stents reduce restenosis in ApoE$^{-/-}$ mice. a) Graphical overview of mouse surgery. A SS stent (without or with HPG coating) was inserted retrograde up the thoracic aorta of an ApoE$^{-/-}$ donor mouse. The aorta was harvested and ligated into the carotid artery of a recipient ApoE$^{-/-}$ mouse. After 28 days of chow diet, the blood vessels containing the stents were removed, fixed, resin embedded, and sections stained with Toluidine blue and Fuchsin. b) In 5 out of 8 controls, stent lumen is completely occluded by neointimal, largely smooth muscle cells, hyperplasia and struts are surrounded by a significant epithelioid macrophage and multinucleated giant cell (foreign body granulomatous) reaction ($n = 8$). By contrast e) the HPG-coated stents have a large patent lumen with minimal neointimal formation. The granulomatous reaction to the struts is greatly reduced compared to controls ($n = 8$). Black structures within the vessels are stent struts. Scale bars indicate 200 µm in images on the left b,e), and 100 µm in the magnified images c,d,f,g). h) Statistical analysis comparing percent occlusion of control and HPG-coated groups, mean ± SEM, $n = 8$ independent experiments. *$p < 0.05$, Student's *t*-test.

through to the coating/substrate interface (as is the case with EtOH plasma polymer coatings).

Bacterial biofilm formation is the primordial reason for the contamination of medical devices. Biofilms are not only resistant to antibiotics and disinfectants, but also facilitate bacteria to evade immune defense mechanisms, such as phagocytosis by macrophages resulting in the persistence of bacteria in the system. Chronic bacterial infections are difficult to treat, which may lead to multiorgan dysfunction and development of cancer. Testing with a range of Gram positive and Gram negative bacteria, including *E. coli, S. aureus, P. aeruginosa, A. baumannii, S. epidermidis*, shows that the HPG coating provides a significantly lower degree of bacterial attachment compared to uncoated substrates. FTIR data also show that, even where bacterial colonization occurs, there is a delay in biofilm formation. The data further corroborate the hypothesis that HPG coatings could be highly suitable for hemocompatibility and non/low-biofouling applications. To further test the applicability of our coating in these areas, we applied HPG to vascular nitinol stents.

Platelet adhesion and activation on implanted stents play a key role in ST and ISR. We were able to show that our HPG coating, when applied to various substrates, significantly reduced platelet binding by >99%. This was confirmed using platelets isolated from fresh human blood on both simple, flat surfaces as well as more complex structures, in a static model. Using the Chandler loop model to simulate blood flow, we showed that when applied to sections of a commercial nitinol stent, the HPG coating dramatically reduced the formation of clots on the stents compared to the uncoated sections. This was consistent across multiple experiments using different donor blood. When the surfaces were examined under high power magnification the lack of any attached and activated platelets or a fibrin network on the HPG-coated stent struts supported the lack of platelet binding observed in the initial static experiments.

Downstream effects of implanted materials that do not manifest at the site of the device are more difficult to correlate with a foreign-body-response but still pose a great risk to patients.[95] Two such effects are the activation of complement and neutrophils. The complement pathway can lead to thrombosis at the site of the device but can also trigger downstream effects through the generation of activated soluble factors that cause inflammatory responses in multiple organs with the kidneys being particularly susceptible to injury.[96] Similarly, neutrophil activation leads to the release of large quantities of ROS that can have devastating effects, such as vascular inflammation, atherosclerosis, and even neurodegeneration.[97–99] When fresh human blood exposed to the HPG-coated stents was further analyzed for evidence of activation of complement or neutrophils, the results showed

our HPG coating could meet these hemocompatibility requirements.

Another key element to the foreign-body-response is inflammation, both acute and chronic, driven by the response of inflammatory cells, such as monocytes and neutrophils, to implanted device.[100] Migration of immune cells and fibroblasts to a wound site is a normal and necessary part of healing. However, implanted materials often disrupt this cycle of tissue repair leading to an imbalance of cell signaling factors and the continued influx of immune cells. Long-term effects may entail fibrous encapsulation of the device if matrix remodeling fibroblasts receive cues due to the presence of the implant. This is particularly problematic with synthetic polymers, even those commonly used in modern day surgical procedures, such as polypropylene mesh for hernia repair,[101] and silicone for breast implants.[102] To this end, it is critical to establish if the addition of the synthetic HPG coating triggers acute or chronic inflammation when implanted into tissue. This broader biocompatibility of the HPG coating was assessed using subcutaneously implanted nitinol disks that were coated and left for up to 5 weeks. The lack of any gross or microscopic evidence of an inflammatory response to either the bare nitinol or HPG-coated nitinol further illustrated the safety of this coating to the surrounding tissue. The same HPG polymer has been shown to be very safe in acute and chronic systemic toxicity studies in small rodents, which has been summarized in several recent reviews.[44,103] Our results confirms that HPG grafted onto surfaces displays similar positive attributes of bio- and hemocompatibility when exposed to human blood, ex vivo.

Apart from ST, ISR can also reduce long-term stent patency. Restenosis is primarily caused by an inflammatory response as a result of stent deployment that stimulates the over-proliferation of medial (vessel wall) smooth muscle cells.[12–14,19,20] DES have significantly helped to overcome this clinical problem and are effective at reducing ISR, however limitations of DES have been documented over the years.[21,104,105] For example, in peripheral arterial disease, the benefits of drug coated devices have not been as dramatic as in coronary arterial disease, with the incidence of ISR in DES beyond 12 months returning to levels similar to bare metal stents.[105] Recent reports also suggest an increased risk of late all-cause mortality and amputations in patients treated with paclitaxel-eluting devices.[23,25] With platelets playing a crucial role in ISR,[12,18] our results with reduced platelet binding on HPG surfaces strongly suggested that our coating could also help prevent the onset of restenosis. In the established mouse model of ISR, we showed a substantial reduction in neointimal restenosis within the stented vessels of the HPG stent. While better understanding the mechanism of action is an area of ongoing research, the result is strongly suggestive of the benefit of our HPG coating to substantially reduce or prevent the cascade of inflammatory responses triggered by the insertion of stents that can lead to ISR.

We note a number of limitations to our study. While we have used XPS to compare the substates before and after the HPG polymerization process, we have not explored the specific chemical reactions that are involved during the polymerization process itself. For further information as to the expected chemical reactions involved in the coating process, we refer back to a number of comprehensive studies in the literature.[51,52,106]

Our AFM data is limited to Si and TiSi substrates (AFM of the coating on rougher substates proved difficult to quantify). While the biological data corroborate the evidence suggesting coatings are uniform and lack gaps or delaminations across a wider range of substrates, we cannot confirm that this would be the case across every substate, and it is possible that some fragile polymer substates may not stand up to the plasma activation step of the coating process, or the subsequent polymerization process at 80–100 °C. However, plasma processes are broadly accepted to produce pinhole free coatings,[107] so we expect that the HPG coating process would produce similar results across a majority of materials.

Based on our measurements, we cannot determine whether the protein adsorbed to the surface during single protein adsorption experiments is a monolayer or aggregate. However, based on the reversibility of protein on HPG, it is most likely in the form of conformationally intact polymers. Our single protein studied are inevitably not as complex a process as would be encountered in vivo or even in ex vivo testing; our experiments therefore do not account for redistribution of proteins via the Vroman effect, where we would expect abundant serum proteins to absorb initially, followed by a redistribution of proteins dependent on each protein's affinity for the surface. However, the both the platelet attachment and chandler loop results indicate that, even in much more complex ex vivo conditions, protein attachment is low.

Finally, our in vivo stent model is one that predominantly assesses inflammation-induced neointimal hyperplasia. The in vitro and ex vivo data show that the HPG coating reduces blood clotting and does not increase inflammation. While the ability of the HPG coating to reduce platelet activation is a pathway to reducing inflammation, we note that there are many more inflammatory pathways that contribute to in-stent neointimal hyperplasia.

In summary, HPG coated vascular stents exhibit greatly improved biocompatibility and hemocompatibility when compared to bare metal substrates. Providing innate compatibility onto existing medical devices could alleviate dependence on pharmacological intervention that currently accompanies all device implantations. Furthermore, such properties could extend the efficacy of devices used in the treatment of peripheral arterial disease, for which current devices suffer high failure rates. This nonbioactive, antithrombogenic, coating could open a new category of stent which maintains the affordability of bare metal stents yet provides superior performance that could rival or outperform DES over the long term. As the polymer is covalently bound to the stent surface this alleviates issues with delamination encountered by dip and spray coating techniques.[108]

4. Conclusion

We have developed a simple, environmentally friendly and commercially viable HPG coating process that is applicable to a wide range of materials via a plasma-activation process. We demonstrate that the coating resists irreversible protein binding and reduces bacterial colonization and biofilm formation. We show that HPG coated vascular stents exhibit greatly improved biocompatibility and hemocompatibility compared to bare metal stents. In addressing the viability of our HPG coating, we investigated the robustness and stability of the coating on commercial stents. The

initial results strongly suggest that our HPG coating can be applied uniformly to the surface of commercial metal stents in a reliable and consistent manner. The coating can withstand the normal manufacturing processing of a commercial stent, from coating through to the final sterile, packaged product. Furthermore, the coating has demonstrated stability up to 44 months, which suggests that a finished product with our coating would have adequate shelf-life stability to meet industry requirements.

The use of bare metal and drug-eluting stents has revolutionized the treatment of cardiovascular and peripheral vascular disease. Even so there remain significant unmet needs in the use of stents for delivering safe and durable relief for patients with vascular occlusions. The industry continues to advance stent technology, seeking new approaches that can promote reendothelialization and avoid restenosis without the need for cytotoxic agents. Similarly, the use of short and long-term implantable devices like catheters and orthopedic, trauma and dental implants are plagued by the formation of bacterial biofilm on their surfaces. Once formed, such biofilms contribute to chronic periprosthetic infections that are difficult to treat and lead to eventual failure of the implant, with increased morbidity and mortality. HPG coating on implantable devices and on tubing used in medical devices is a promising way to prevent hospital acquired infections. It could also be used in industrial settings to prevent microbial contamination.

Collectively, these complications reduce a patient's quality of life and add considerably to national healthcare budgets. Through rigorous testing we have demonstrated in laboratory tests that our novel HPG coating has the qualities and properties of a truly biocompatible coating with tremendous potential to improve the performance, safety and durability of a broad range of devices.

5. Experimental Section

HPG Sample Preparation—Coating of HPG Coated Substrates for Study of Coating Process: For studies of the HPG coating process, as well as protein adsorption and *S. epidermidis* microbiology work, HPG-grafted Si, TiSi, PTFE, Al, and glass, fixed to 1×1 cm^2, and nitinol stents, fixed to $1 \times 1 \times 1$ cm^3, were prepared as follows. Substrates were gently agitated in 100% isopropanol (Thermo Fisher Scientific) for three 5 min washes. Substrates were then dried under a stream of N_2 and activated with air plasma in a Diener Electronic Zepto plasma cleaner. Plasma activation was carried out under application of continuous LF power of 100 W for 20 min, with 4 sccm flow rate of air. Following plasma treatment, the vacuum chamber was backfilled with air and the substrates immediately immersed in distilled glycidol and left to polymerize in an oven at 80 °C for 24 h. Polymerization was terminated by removing the unreacted monomer solution and quenching the reaction by a succession of three 5 min washes with methanol under light agitation. HPG-grafted substrates were dried under a stream of N_2 and stored under ambient conditions until use.

Coating of HPG Coated PS Substrates for Biological Analysis: For HPG-grafted PS samples, silicon wafers were cut into 1 cm^2 pieces, and cleaned using the Radio Corporation of America (RCA) critical process guidelines. Samples were treated for 30 min at 70 °C with a 1:1:5 ratio of ammonium hydroxide, hydrogen hydroxide, and MilliQ water, respectively. They were then washed twice with MilliQ water before being immersed and sonicated for 5 min in ethanol followed by acetone. Clean silicon wafers were stored in acetone before use. Before doing the spin coating, a solution 1.75% of PS by weight was made by dissolving PS beads in toluene at 50 °C for 2 h. Silicon wafers were dried with a stream of N_2. Each sample was subsequently coated with 100 µL of the PS solution using a spin coater at the rate of 3000 rpm for 40 s. PS-coated silicon pieces were then activated with air plasma in a custom-built reactor similar to the one described previously.[109]

Plasma activation of PS was carried out under application of continuous RF power of 100 W for 5 min, with air pressure during treatment at 3×10^{-2} mbar. Samples were immediately immersed in distilled glycidol after plasma activation and left to polymerize in an oven at 100 °C for 24 h. Polymerization was terminated by removing the unreacted monomer solution and quenching the reaction by a succession of three 5 min washes with methanol under light agitation. Before further analysis, samples were thoroughly washed with PBS (every 15 min for 3–4 h). An additional washing with MilliQ water was performed for another 2 h and samples were dried with a stream of N_2, if they were to be studied for surface analysis.

Coating of HPG Coated TiSi, SS Mesh, Nitinol Stents, Nitinol Sheet, and SS Mouse Stents for Biological Analysis: Except where indicated, HPG-grafted TiSi, SS mesh, nitinol stents, nitinol sheet, and SS mouse stents were prepared as follows. Substrates were gently agitated in 100% isopropanol (Thermo Fisher Scientific) for three 5 min washes. Substrates were then dried under a stream of N_2 and activated with argon plasma in a Diener Femto plasma cleaner. Plasma activation was carried out under application of continuous LF power of 100 W for 20 min, with argon pressure during treatment at 6×10^{-2} mbar. Following plasma treatment, the vacuum chamber was backfilled with argon gas and the substrates immediately immersed in distilled glycidol and left to polymerize in an oven at 100 °C for 24 h. Polymerization was terminated by removing the unreacted monomer solution and quenching the reaction by a succession of three 5 min washes with methanol under light agitation. HPG-grafted substrates were dried under a stream of N_2 and stored under ambient conditions until use. Samples prepared in this manner were used for all blood contact work, in vivo mouse studies and *E. coli*, *S. aureus*, *P. aeruginosa*, and *A. baumannii* microbiology work.

Plasma Polymerization of Ethanol: Plasma polymerization (PP) was conducted in a clean glass barrel reactor connected to a vacuum pump (maintaining 0.38 Pa base pressure) and a 13.56 MHz radiofrequency (RF) generator (Coaxial Power System Ltd, UK). To coat Si with ethanol, monomer (5 mL) was pipetted into a round bottom flask connected to the plasma chamber. A piece of substrate (Si) was placed in the glass chamber and the whole system was brought to base pressure. By opening the monomer inlet valve, the pressure of the plasma reactor was increased to 10 Pa, at which point the RF power was switched on and maintained at 30 W when the plasma ignited. Conditions were maintained (4.67 sccm flow rate) for 15 min to allow plasma deposition. Once complete, RF power was switched off and the chamber allowed to stabilize for 1 min after which the chamber was returned to atmosphere and the coated substrate removed.

XPS: XPS was performed using two separate spectrometers at Lancaster University (UK) and the University of South Australia. XPS in Sections 2.1 and 2.2 (at Lancaster University), for the study of the coating process and protein adsorption work, was performed using a Kratos AXIS Supra spectrometer (Kratos Analytical Ltd, Manchester, UK), using monochromatic Al Kα radiation ($h\nu = 1486.7$ eV). Samples were mounted on sample holder using double sided Kapton tape and an internal flood gun was used to reduce charging effects. Spectra were recorded using an acceleration voltage of 15 keV at a power of 225 W. Samples were measured in triplicate with a take-off angle of 90°. Wide scan survey spectra were collected in three locations per sample with a pass energy of 160 eV, a step size of 1 eV, a sweep time of 120 s and an analysis area of 300×700 µm^2. High-resolution core line spectra were obtained in 3 locations per sample using a 20 eV pass energy, a step size of 0.1 eV, a sweep time of 120 s, and an analysis area of 300×700 µm^2.

XPS in Section 2.3 (at University of South Australia), for samples prepared for biological testing, was performed with a Kratos AXIS Ultra DLD spectrometer, using monochromatic Al Kα radiation ($h\nu = 1486.7$ eV). The system is equipped with a magnetically confined charge compensation system (low energy electrons are confined and transported to the sample surface by magnetic field). Spectra were recorded using an acceleration voltage of 15 keV at a power of 225 W. Wide scan survey spectra were collected with a pass energy of 160 eV and an analysis area of 300×700 µm^2.

High-resolution core line spectra were obtained using a 20 eV pass energy and an analysis area of 300 × 700 μm^2.

Data analysis was performed with CasaXPS software (version 2.3.22, Casa Software Ltd, Devon, UK). All binding energies were referenced to the low energy C 1s peak at 285.0 eV. Core level envelopes were curve-fitted with the minimum number of mixed Gaussian–Lorentzian component profiles. The Gaussian–Lorentzian mixing ratio (typically 30% Lorentzian and 70% Gaussian functions) the full width at half-maximum, and the positions and intensities of peaks were left unconstrained to result in a best fit.

XPS Depth Profiling: XPS ion milling was performed with an Axis Supra spectrometer, using an argon gas cluster source with 2000$^+$ cluster size and 5 keV energy. Over a 4 mm raster, 100 etches were milled with pre-etch, etch, and post-etch time each fixed at 10 s. Samples were rotated 90° between each etch step. Core-line spectra (C 1s, O 1s, N 1s, Si 2p, and Ti 2p) were collected, where relevant, using a 110 μm slot size, an acceleration voltage of 15 keV, emission current of 25 mA (operating power = 375 W), pass energy of 40 eV, step size of 0.1 eV, and a 60 s sweep time.

End Group Labeling: Samples were placed inside a vacuum chamber and pumped to the base pressure (0.5 Pa). TFAA, (>5 mL) was pipetted into a round bottom flask which was attached at the monomer inlet of the chamber. The inlet valve was opened and the TFAA was heated to 40 °C in a water bath to increase the pressure inside the reactor chamber to 700 Pa. Samples remained in the chamber for 1 h before closing the monomer inlet valve and maintaining system pumping for a further 30 min, to remove surplus TFAA. Samples removed and stored under vacuum until XPS analysis.

AFM: AFM images were collected using a Bruker Multimode 8 AFM equipped with a Nanoscope V controller operated in the PeakForce mode at ultralow noise facility at Lancaster University, IsoLab. NuNano Scout 70 probes were used with a nominal resonant frequency of 70 kHz, 2 N m^{-1} cantilever stiffness, and less than 10 nm probe radius. The AFM was calibrated using atomic steps on highly oriented pyrolytic graphite and Au (111). To measure the polymer thickness, the coating was scratched in contact mode in a 500 nm × 500 nm area. The thickness was estimated from the difference in the height inside and outside the scratched area using a line profile and height histogram analysis.

Protein Adsorption Test: Samples were placed in a well plate and prehydrated in phosphate buffer saline (PBS, 0.01 M, 1 mL), for 30 min. Albumin and fibrinogen (2 mg mL^{-1}) were added individually to sample wells, before incubating (static, room temp.) for 1 h. Samples to measure reversibly bound protein were washed with PBS (three times, 1 mL) following incubation. To determine irreversibly bound protein samples were first incubated in SDS solution for a further 72 h before the standard PBS wash (three times, 1 mL). After simple or SDS washing and sample drying, the samples XPS measurements were collected. The nitrogen content on the surface was used as a measure of adsorbed protein. To allow direct comparison between results, N counts were normalized to Au counts measured on a gold standard (Au on mica) on each day of data point collection.

Microbiology and Biofilm Testing—E. Coli, S. Aureus, P. Aeruginosa, and A. Baumannii: Bacterial strains (*P. aeruginosa* (ATCC 27 853), *S. aureus* (ATCC 29 213) *E. coli* (ATCC 25 922), and *A. baumannii* ACICU) were streaked onto a Luria–Bertani (LB) agar and incubated for 24 h at a 37 °C incubator. For each experiment, 3 single colonies were picked and inoculated into 3 mL Luria–Bertani (LB) broth. The cultures were grown aerobically for 16–18 h at 200 rpm at 37 °C using a rotary shaker. The overnight cultures were diluted to 0.1 OD_{600} in LB broth, and 1 mL of the culture was added on top of the uncoated and HPG-coated TiSi wafers in a Falcon 24 Well Clear Flat Bottom. Wafers exposed to bacteria were identical in size (10 mm × 10 mm) and surface area. This resulted in a surface-area-to-volume ratio of 0.227. The culture plates were incubated at 37 °C standard incubator for static and in a rotary shaker for the rotary culture studies for 24 h.

Standard crystal violet staining was used to analyze the biofilm growth. Static and rotary cultures were removed from the wafers and washed 5 times with sterile distilled water to remove loose and weakly bound biofilms. Then the biofilms were fixed and stained in 0.5% Crystal Violet blue in 20% methanol for 30 min at room temperature. The excess stain was washed off with water and air-dried overnight at room temperature prior to imaging with bright field microscopy.

The biofilm mass was analyzed by DAPI staining for bacterial nuclei. Static and rotary cultures were removed from the wafers and washed 5 times with PBS to remove loose and weakly bound biofilms. The biofilms were fixed with 4% Paraformaldehyde in PBS for 20 min at room temperature. The fixing solution was removed, and the wafers were washed three times with PBS. Finally, the wafers were mounted with Prolong Diamond containing DAPI using a coverslip and air-dried overnight at room temperature in the dark. The DAPI-stained biofilms were analyzed using Zeiss LSM 800 confocal microscope, and images were analyzed in ImageJ.

The amount of viable biofilm on wafers was analyzed by standard CFU assay. In brief, the static and rotary cultures were removed from the wafers and washed 5 times with sterile distilled water to remove loose and weakly bound biofilms. Then the wafers were transferred to a fresh 24-well dish, and 1 mL sterile distilled water was added. The biofilms were scraped from the wafers and flushed vigorously into the 1 mL water. The wafer was stained with crystal violet to ensure effective removal of biofilm from the wafers. The samples were serially diluted (from 10^0 to 10^5), and 100 μL of each dilution was spread plated on LB agar aseptically. The media plates were incubated overnight at 37 °C. Colony-forming units (CFUs) were recorded and plotted using Graph pad PRISM.

S. Epidermidis: Surface biomass was evaluated after 24–72 h of incubation with *S. epidermidis* (ATCC 35 984), starting with a bacterial concentration of 3 × 10^7 CFU mL^{-1}. Following incubation, a serial dilution, Miles and Misra, was performed to quantify the biomass on the surface. A novel application of FTIR was also applied to define whether a biofilm had formed on the sample and control surfaces. Following incubation to grow bacteria, samples removed from solution and transferred to an isolated desiccant chamber for 30 min. Samples analyzed with FTIR immediately following drying. Planktonic samples analyzed as a control in a similar way by looping onto clean sample and isolating for 30 min in desiccant chamber before spectra collection.

Fluorescence Microscopy Live Dead Stain (S. Epidermidis): Samples (HPG on glass slides) were incubated in bacterial culture media and biofilm formation of *S. epidermidis* was facilitated as described above. Following 4 h incubation samples were removed from culture media and washed with PBS (1 mL). To produce staining mixture, combine calcofluor white (1.5 μL per 1 mL PBS, 1 g L^{-1}, Fluka analytical), propidium iodine (1.5 μL per 1 mL PBS, 0.1 mg mL^{-1}, Life technologies), and Syto9 (1.5 μL per 1 mL PBS, 5 mM, Invitrogen). Add dye mixture (35 μL) to each sample and cover with glass coverslip. Incubate in the dark for 30 min. Remove coverslip and wash cells with PBS (1 mL, three times) then add 4% paraformaldehyde (50 μL), cover with a coverslip and incubate in the dark for 15 min. Once ready to complete the imaging, remove sample from coverslip and mount in a new 6-well plate on a drop of BacLight mounting medium (Invitrogen). Image sample with Invitrogen EVOS M5000 microscope x40 objective (calcofluor white (blue filter), Syto9 (green filter), and propidium iodide (red filter)).

FTIR of Biofilm Formation: A desktop Summit PRO FTIR spectrometer (Nicolet, Thermo Scientific, UK) with iD1 transmission sampling apparatus was used for all analysis. Data was collected using OMNIC Paradigm software (Thermo Scientific, UK). Data acquisition was performed at 4 cm^{-1} resolution, accumulating 64 scans over a spectral range of 4000–800 cm^{-1}. Each sample was repeated in triplicate. Data analysis was conducted using OMNIC software in the first instance. Each spectrum was processed in the same way, completing normalization followed by a base line correction.

SEM: Fixed stents were dehydrated (80% EtOH 24 h, 90% EtOH 24 h, 100% EtOH 24 h) and dried (50:50 solution of EtOH and Hexamethyldisilazane (HDMS, Sigma-Aldrich) for 20 min and finally 100% HMDS for 20 min prior to air drying) prior to sputter coating with 10 nm platinum in a Cressington 208 HR sputter coater (Cressington, Watford, UK) using an Argon (BOC, North Ryde, Australia) plasma and platinum sputter target (ProSciTech, Thuringowa Central, Australia). Samples were examined under a SEM (Crossbeam 540 with GEMINI II column, Carl Zeiss, Oberkochen, Baden-Wurttemberg, Germany) equipped with a field emission gun operated at 3 kV, a 100 pA probe current applied and

secondary electron images recorded with an Inlens Secondary Electron detector.

Ethics: The collection of peripheral blood from healthy individuals was approved by the Human Research Ethics Committees (HREC) of the Royal Adelaide Hospital (#130 308 and #201 187), the University of South Australia (#200 585) and the University of New South Wales (HC14108). Animal studies were approved by animal ethics committees of SA Pathology & University of South Australia (#18-16) as well as the South Australian Health and Medical Research Institute (SAHMRI, #SAM422.19).

Isolated Platelet Assays: Platelet assays on flat PS were performed with the help of Dr Jelena Rnjak-Kovacina and Kieran Lau at the University of New South Wales (UNSW) and were approved by the ethics board (HC14108) of UNSW (Australia).

Blood was collected from a healthy donor, put in vacutainers containing 3.2% trisodium citrate as an anti-coagulant (Becton Dickson, Macquarie Park, NSW, AU) and used straight away. The upper platelet-rich plasma was aspirated after a 160 g centrifugation for 15 min and centrifuged again at 340 g for 15 min. The platelet pellet was then resuspended in Tyrode's buffer (Sigma-Aldrich, St Louis, MO) with 0.1 U mL^{-1} apyrase. Particular care was given to limit any shear stress and agitation in order to prevent platelet activation during the isolation process. Platelets were seeded at 5×10^6 platelets per well onto each sample material and incubated for 1 h at 37 °C. Platelets were fixed with 4% paraformaldehyde solution with 1% sucrose for 15 min, and then permeabilized with 300 mM sucrose, 50 mM NaCl, 3 mM $MgCl_2$, 2 mM HEPES, 0.5% Triton X-100, pH 7.2 for 5 min at 4 °C and blocked in 1% BSA in PBST (PBS containing 0.05% Tween-20) for 1 h at room temperature. Two PBS washes were performed between each of the above steps. Samples were stained with rhodamine phalloidin (Life Technologies, Carlsbad, CA) at 1:200 dilution ratio for 1 h at 37 °C. Finally, samples were rinsed twice with PBST, before being fixed onto a glass slide with a droplet of Fluoromount aqueous mounting medium covered by a glass coverslip deposited on each sample. Samples were stored in the dark before imaging.

Platelet assays on SS mesh was performed with the help of Dr. Carmela Martini (University of South Australia). Blood from healthy donors (aged 18–65 years, nonsmokers and aspirin/NSAIDs free for at least 1 month) was collected into acid-citrate dextrose (ACD, pH 4.5) anticoagulant and platelets purified as described elsewhere.[110] Briefly, blood was collected from single donors, rested at RT for 15 min prior to 180 g centrifugation, the platelet-rich-plasma was then centrifuged at 1100 g for 15 min and the platelet pellet was resuspended gently with Tyrode's platelet wash buffer (137 mM NaCl, 2.7 mM KCl, 1 mM $MgCl_2.6H_2O$, 12 mM $NaHCO_3$, 0.4 mM $NaH_2PO_4.H_2O$, 3.7 mM HEPES, pH 7.4) containing 1.78 U mL^{-1} Apyrase (BD Biosciences, San Jose, CA). The platelet suspension was incubated at 37 °C for 5 min, centrifuged at 1100 × g for 15 min then resuspended in Tyrode's platelet resuspension buffer (Tyrode's wash buffer, 3 mM $CaCl_2$) containing 0.178 U mL^{-1} Apyrase. Platelets were counted using a Sysmex XE-5000 differential analyzer (Sysmex Corporation, Kobe, Japan) and validated for purity and low-level activation via flow cytometric analysis. Platelets were stained with anti-CD42b and anti-CD62P or isotype-matched control antibody (all BD Biosciences, Ann Arbor, MI) for 15 min with samples processed by a BD Accuri C6 flow cytometer with subsequent analyses performed on FCS Express 6 cytometry software (De Novo Software, Glendale, CA).

Platelets were seeded at 3×10^6 platelets per well, in platelet suspension buffer, onto each sample material and incubated for 2.5 h at 37 °C. Samples were then washed lightly once with PBS and fixed with paraformaldehyde (4% in PBS) for 15 min at room temperature. Three PBS washes were performed following fixing of the samples then adhered platelets were stained with CFDA SE cell tracer (Thermo Fisher Scientific) at 1:2000 dilution ratio for 20 min at 37 °C. Finally, samples were rinsed three times with PBS and three times with MilliQ water then stored in the dark before imaging.

Chandler Loop Assay: Nonpackaged stent sections, both control and HPG-coated were rinsed in RO water three times for 5 min each and then sterile PBS three times for 5 min each in a biosafety cabinet. Washed samples were removed from the PBS and placed individually into lengths of Tygon ND-100-65 tubing. Crimped, packaged and ethylene oxide (EO) sterilized full-length stents were stored at room temperature for up to 44 months prior to being deployed directly into the Tygon tubing from the catheter in a biosafety cabinet. The tubes were sealed in a loop using an out cuff that held the two ends firmly together. Sticky tape was also applied to the ends of the cuff to ensure it did not come apart. Each tube was slid over a plastic container that acted as the drum of the rotator and taped in place. A 19G and 26G needle were placed into each tube to enable blood to be injected in (19G) while allowing air to escape (26G).

50 mL of healthy human blood was collected in the lab into a syringe preloaded with Heparin (0.5 U mL^{-1} blood) diluted into 1 mL PBS. The blood was injected into the loops within 2 min of collection, leaving an ≈2 cm long air bubble at the top of each loop. Needles were removed from the loops and tape was applied over the puncture sites to prevent leakage. The loops were rotated at 175/s (≈5 dyn cm^{-2}) for 2–4.5 h, at 37 °C. At the conclusion of the assay, loops were cut open and the contents of each was collected. Clots in stents was blotted on paper to remove liquid blood and placed in preweighed tubes. Stents with little or no clot were dipped in PBS 5 times to remove unbound blood before being blotted dry on paper towel and placed in preweighed tubes. The weight of each stent and associated clot was recorded. Stents were then cut away from protruding clots and all devices were fixed in PFA over night at room temperature. Following fixation, stents were washed once with PBS, once with RO water and then placed in ethanol (80% V/V).

Complement and Neutrophil Activation: Complement and neutrophil activation assays were performed by SA Pathology as a fee for service following accredited protocols outlined in internal documents PRC-IMI-020-REV2 and PRC-IMP-157, respectively. In short, complement activity was measured from healthy donor serum collected fresh for this assay and compared to a reference sample of pooled serum provided by SA Pathology using the CH50 assay. Neutrophil activation was measured from isolated cells using the dihydrorhodamine-123 oxidative burst assay with phorbol myristate acetate (PMA) added to one sample as a positive control. For each of 5 healthy donors, of various age and sex, 5 × 9 mL blood was collected in Vacuette lithium heparin tubes. One tube of blood was retained as a native blood control that had not been subjected to the Chandler loop conditions. The remaining four tubes were combined, and 10 mL of heparinized blood loaded into 3 prepared loops as described above for the Chandler loop assay. One loop contained no stent sample and acted as a control for activation via handling, exposure to the tube material and flow conditions. The two remaining loops contained either a bare control stent or a HPG coated stent. All three loops were sealed and run as described previously for 1 h. Following exposure for 1 h, the blood was collected from the loops and taken, at room temperature, for testing. All testing was performed within 2.5 h of collection from donors.

In Vivo Inflammatory Response Model: Female Balb/c mice aged 6–8 weeks were sourced from the Animal Resource Centre (Perth, Australia), and housed under conventional conditions. A 1 cm incision was made in the skin along the midline of the back and blunt dissection was used to create a pocket under the skin on each flank for disk. Each mouse received an HPG-coated and bare uncoated nitinol disk 5 mm in diameter under the skin of each flank with sides randomized. For the coated disks the coating side was placed facing the skin. After checking disk placement, the midline incision was closed with 4.0 chomic gut sutures (Dynek, Hendon, SA, Australia). Disks remained embedded for either 1 or 5 weeks. At the endpoint, the skin above each disk was inspected for signs of inflammation and the disk was removed along with the skin in contact with the disk, ≈10 × 10 mm^2. Skin sections were fixed in 10% buffered formalin (Bio-Strategy Ltd, Auckland, New Zealand) and paraffin embedded.

Formalin fixed paraffin embedded skin sections were cut to 8 µm, dewaxed and stained with hematoxylin and eosin to show skin morphology and signs of inflammation. Stained slides were scanned on a NanoZoomer 2.0-HT (Hamamatsu, Japan) and blinded before analysis with NDP.view software (Hamamatsu). Measurements were taken of the width of the Epidermis, dermis, muscle, and adipose layers along with the full skin thickness at two separate points on the section for 2–4 separate sections of skin per mouse. Results were analyzed and graphed in Prism (Graphpad, CA) and compared to back skin from normal Balb/c mice that did not receive a disk or surgery.

Carotid Interposition Graft Model of Stenting: The surgical procedure was performed as previously described.[89,111] In chow-fed, 10- to 14-week-old male ApoE$^{-/-}$ donor mice, a SS stent (2.5 × 0.6 mm; Brivant Ltd., Galway, Ireland) was crimped onto a 1.25 × 0.6 mm balloon angioplasty catheter (Medtronic, Milwaukee, Wisconsin). This was inserted retrograde up the thoracic aorta of the donor mouse through a small transverse arteriotomy made marginally superior to the diaphragmatic outlet and the balloon inflated to an atmospheric pressure of 12 Pa for 30 s. The aorta (≈10–15 mm in length) was harvested by sealing the intercostal branch vessels with electrocautery. The harvested aortas did not exceed a total ischemic time of 15 min and were stored in PBS.

In the recipient mouse, the right common carotid artery was ligated and divided between 7-0 silk ties at its midpoint. Polyethylene cuffs (0.65 mm diameter) were placed over each end and anchored by clamps. The artery was everted over the cuffs and secured with 8-0 silk sutures. The donor aorta was then interposition-grafted by sleeving its ends over the carotid artery cuffs and secured using 8-0 silk sutures. Vessel patency was checked by removing the clamps and restoring blood flow to the vessel. Mice received aspirin (10 mg kg^{-1} day^{-1}) in drinking water for 1 week before surgery and postsurgery for 28 days to reduce the risk of in-stent thrombosis.

Resin Embedding of Stented Vessels: Stented vessels were harvested 28 days after surgery and perfused in situ with 4% phosphate-buffered paraformaldehyde, then excised and embedded into JB-4 (glycol methacrylate) resin (ProSciTech, Thuringowa Central, Australia) according to the manufacturer's instructions for histomorphometry and immunohistochemistry analysis. Transverse sections (5 µm) of the stent were cut using a tungsten-carbide blade on an automatic microtome.

In-Stent Neointimal Hyperplasia Quantification

For histomorphometric analysis, resin-embedded samples were stained with Toluidine blue and Fuchsin then imaged on a Hamamatsu Photonics NanoZoomer whole slide imaging microscope. The total neointimal area was quantified in NDP.view 2 software on 5 stented sections/vessel by taking the area inside the internal elastic lamina, minus, the lumen. An additional measurement was performed that looked at the stent strut to the edge of the lumen distance (4–6 measurements per section).

Statistical Analysis: XPS data throughout are presented as the mean of three measurements (three separate sample locations on each sample) ± standard deviation. For XPS CPS values for protein work (Section 2.2.1., and Figure S8, Supporting Information), N counts were normalized to Au counts measured on a gold standard (Au on mica) each day of data point collection. Data displayed in Figure 6b: Bars represent the mean with dots of individual experiments, ****$p < 0.0001$, Student's *t*-test. CFUs recorded and plotted using Graph pad PRISM. Data displayed in Figure 7b: Data represent mean ± SEM,**** = $p \leq 0.0001$ unpaired Student's *t*-test. Analyses performed on FCS Express 6 cytometry software (De Novo Software, Glendale, CA). Data displayed in Figure 8c: Data represent mean ± SEM, $n = 12$ independent experiments, ** = $p \leq 0.01$, Student's *t*-test. Data displayed in Figure 9: Data represent mean ± SEM, $n = 5$ independent donors, ** = $p \leq 0.01$, unpaired Student's *t*-test. Data displayed in Figure 10b: Data represent mean ± SEM, $n = 3$–15 mice, * = $p \leq 0.05$, ** = $p \leq 0.01$ unpaired Student's *t*-test. Data displayed in Figure 10d,e: Data represent mean ± SEM, $n = 3$–15 mice, * = $p \leq 0.05$, ** = $p \leq 0.01$ one-way ANOVA. Data displayed in Figure 11: data represent mean ± SEM, $n = 8$ independent experiments. *$p < 0.05$, Student's *t*-test. Data quantified in NDP.view 2 software.

Supporting Information

Supporting Information is available from the Wiley Online Library or from the author.

Acknowledgements

This work was funded by grants awarded to C.S.B. by the CRC for Cell Therapy Manufacturing (CRC CTM), as well as funding to C.S.B. and E.M. from TekCyte Limited (a spin-out company from the CRC CTM), to C.S.B., P.J.P., and E.M. from the National Health and Medical Research Council Development Grant (No. GNT1175142) and to E.M. from the National Heart Foundation Australia and a Mary Overton Fellowship from the Royal Adelaide Hospital Research Fund. A.J.R., A.C., A.Q., S.P.J., I.U.R., and R.D.S. acknowledged funding from the European Regional Development Fund through the Greater Innovation for Smart Materials Optimization (GISMO) Project (Grant Reference No. 03R18P02671). A.J.R. acknowledged funding from the Joy Welch Educational Charitable Trust. R.D.S. acknowledged funding from the Engineering and Physical Sciences Research Council (Nos. EP/S004505/1 and EP/V00607X/1). The authors would like to thank Mark Butcher and Jontana Allkja at Glasgow University for their assistance with Fluorescence microscopy live dead stain experiments, Dr. Carmela Martini, Dr. Jelena Rnjak-Kovacina, and Kieran Lau for assistance with platelet isolation and experiments, and Samantha Escarbe for histological assistance. Figure illustrations were created with BioRender.com.

Conflict of Interest

T.S. is the CEO and shareholder of TekCyte Limited, which is commercializing HPG coatings. E.M. was employed 0.2 FTE by TekCyte Limited. E.M., C.S.B., G.B., and N.H.V. are inventors on patents involving the HPG coating process (Nos. WO2017156592 and WO2017156593). C.S.B., E.M., M.P.C., G.B., and R.S. are shareholders in TekCyte Limited. All other authors have nothing to declare.

Author Contributions

E.M. and A.J.R. contributed equally to this work. E.M., N.H.V., H.J.G., T.S., G.B., C.S.B., and R.S. conceived the study. E.M., A.C., A.B., M.P.C., R.G., N.R., and S. A.-B. designed, performed, and analyzed the experiments, interpreted data and generated figures. M.P.C., L.S., and V.N. performed in vivo experiments. M.P.C. collected human blood. L.M. performed end-group labeling experiments. A.Q. and S.P.J. performed and interpreted AFM experiments. R.G., N.R., G.R., and A.C. designed and performed fluorescence microscopy live-dead stain experiments. C.W., I.U.R., and A.C. conceived FTIR experiments. M.T., P.J.P., J.W.F., and T.S. interpreted data. C.S.B., C.B., H.J.G., N.H.V., A.J.R., and R.S. designed experiments and interpreted data. E.M., M.P.C., A.J.R., and M.T. generated figures. E.M. and A.J.R. wrote the manuscript with input from all authors.

Data Availability Statement

The data that support the findings of this study are available from the corresponding author upon reasonable request.

Keywords

biofilms, hyperbranched polyglycerol, in-stent restenosis, nonfouling, peripheral arterial disease, thrombosis, X-ray photoelectron spectroscopy

Received: April 29, 2024
Revised: June 10, 2024
Published online:

[1] E. Mariani, G. Lisignoli, R. M. Borzì, L. Pulsatelli, *Biomaterials* **2019**, *20*, 636.
[2] J. Iqbal, J. Gunn, P. W. Serruys, *Br. Med. Bull.* **2013**, *106*, 193.
[3] G. A. Mensah, V. Fuster, C. J. L. Murray, *J. Am. Coll. Cardiol.* **2023**, *82*, 2350.

[4] W. H. Organisation, https://www.who.int/news-room/fact-sheets/detail/the-top-10-causes-of-death, (accessed: March 2024).
[5] A. Sakamoto, H. Jinnouchi, S. Torii, R. Virmani, A. V. Finn, *Bioengineering* **2018**, *5*, 71.
[6] E. C. L. Grove, S. D. Kristensen, *E-J. Cardiol. Pract.* **2007**, *5*, 32.
[7] C. Werner, M. Maitz, C. Sperling, *J. Mater. Chem.* **2007**, *17*, 3376.
[8] Y.-H. Li, C.-Y. Fang, I.-C. Hsieh, W.-C. Huang, T.-H. Lin, S.-H. Sung, C.-Z. Chiu, C.-J. Wu, K.-G. Shyu, P.-Y. Chang, C.-C. Fang, T.-M. Lu, C.-P. Chen, W.-C. Tai, C.-C. Sheu, K.-C. Wei, Y.-H. Huang, H.-M. Wu, J.-J. H. Hwang, *Acta Cardiol. Sin.* **2018**, *34*, 201.
[9] S. Degrauwe, T. Pilgrim, A. Aminian, S. Noble, P. Meier, J. F. Iglesias, *Open Heart* **2017**, *4*, e000651.
[10] S. Banerjee, D. J. Angiolillo, W. E. Boden, J. G. Murphy, H. Khalili, A. A. Hasan, R. A. Harrington, S. V. Rao, *J. Am. Coll. Cardiol.* **2017**, *69*, 1861.
[11] J. A. Spertus, R. Kettelkamp, C. Vance, C. Decker, P. G. Jones, J. S. Rumsfeld, J. C. Messenger, S. Khanal, E. D. Peterson, R. G. Bach, H. M. Krumholz, D. J. Cohen, *Circulation* **2006**, *113*, 2803.
[12] A. K. Mitra, D. K. Agrawal, *J. Clin. Pathol.* **2006**, *59*, 232.
[13] F. G. P. Welt, C. Rogers, *Arterioscler., Thromb., Vasc. Biol.* **2002**, *22*, 1769.
[14] A. H. Gershlick, J. Baron, *Heart* **1998**, *79*, 319.
[15] R. V. Tadwalkar, M. S. Lee, *Vasc. Dis. Manage.* **2015**, *12*, e190.
[16] K. M. Sanders, P. A. Schneider, M. S. Conte, J. C. Iannuzzi, *Semin. Vasc. Surg.* **2021**, *34*, 172.
[17] U. Sarwar, M. Nadeem, A. Hussain, N. Bardia, H. Tahir, *Int. J. Cardiol. Cardiovasc. Disorder* **2021**, *2*, 1.
[18] H. Haybar, M. S. S. Pezeshki, N. Saki, *Curr. Cardiol. Rev.* **2020**, *16*, 285.
[19] R. P. Tan, I. Ryder, N. Yang, Y. T. Lam, M. Santos, P. L. Michael, D. A. Robinson, M. K. Ng, S. G. Wise, *Vasc. Dis. Manage.* **2021**, *6*, 693.
[20] M. Maleknia, N. Ansari, H. Haybar, M. Maniati, N. Saki, *SN Compr. Clin. Med.* **2020**, *2*, 397.
[21] B. L. van der Hoeven, N. M. M. Pires, H. M. M. Warda, P. V. Oemrawsingh, B. J. M. van Vlijmen, P. H. A. Quax, M. J. Schalij, E. E. van der Wall, J. W. Jukema, *Int. J. Cardiol.* **2005**, *99*, 9.
[22] A. A. Bavry, D. J. Kumbhani, T. J. Helton, P. P. Borek, G. R. Mood, D. L. Bhatt, *Am. J. Med.* **2006**, *119*, 1056.
[23] K. Katsanos, S. Spiliopoulos, P. Kitrou, M. Krokidis, D. Karnabatidis, *J. Am. Heart Assoc.* **2018**, *7*, e011245.
[24] C.-A. Behrendt, A. Sedrakyan, F. Peters, T. Kreutzburg, M. Schermerhorn, D. J. Bertges, A. Larena-Avellaneda, H. L'Hoest, T. Kölbel, E. S. Debus, *Eur. J. Vasc. Endovasc. Surg.* **2020**, *59*, 587.
[25] T. Zeller, I. Baumgartner, D. Scheinert, M. Brodmann, M. Bosiers, A. Micari, P. Peeters, F. Vermassen, M. Landini, D. B. Snead, K. C. Kent, K. J. Rocha-Singh, *J. Am. Coll. Cardiol.* **2014**, *64*, 1568.
[26] T. Singh, A. L. Hook, J. Luckett, M. F. Maitz, C. Sperling, C. Werner, M. C. Davies, D. J. Irvine, P. Williams, M. R. Alexander, *Biomaterials* **2020**, *260*, 120312.
[27] M. van Kerckhoven, A. Hotterbeekx, E. Lanckacker, P. Moons, C. Lammens, M. Kerstens, M. Ieven, P. Delputte, P. G. Jorens, S. Malhotra-Kumar, H. Goossens, L. Maes, P. Cos, *J. Microbiol. Methods* **2016**, *127*, 95.
[28] C. Potera, *Environ. Health Perspect.* **2010**, *118*, A288.
[29] A. Yousif, M. A. Jamal, I. Raad, *Adv. Exp. Med. Biol.* **2015**, *830*, 157.
[30] H. Toor, S. Farr, P. Savla, S. Kashyap, S. Wang, D. E. Miulli, *Cureus* **2022**, *14*, e22809.
[31] M. Cámara, W. Green, C. E. MacPhee, P. D. Rakowska, R. Raval, M. C. Richardson, J. Slater-Jefferies, K. Steventon, J. S. Webb, *NPJ Biofilms Microbiomes* **2022**, *8*, 42.
[32] A. L. S. Burzava, M. Jasieniak, M. P. Cockshell, N. H. Voelcker, C. S. Bonder, H. J. Griesser, E. Moore, *ACS Appl. Bio. Mater.* **2020**, *3*, 3718.
[33] K. Höger, T. Becherer, W. Qiang, R. Haag, W. Frieß, S. Küchler, *Eur. J. Pharm. Biopharm.* **2013**, *85*, 756.
[34] C. Siegers, M. Biesalski, R. Haag, *Chemistry* **2004**, *10*, 2831.
[35] N. Beshchasna, M. Saqib, H. Kraskiewicz, Ł. Wasyluk, O. Kuzmin, O. C. Duta, D. Ficai, Z. Ghizdavet, A. Marin, A. Ficai, Z. Sun, V. F. Pichugin, J. Opitz, E. Andronescu, *Pharmaceutics* **2020**, *12*, 349.
[36] Z. K. Zander, M. L. Becker, *ACS Macro Lett.* **2018**, *7*, 16.
[37] B. Mendrek, N. Oleszko-Torbus, T. Teper, A. Kowalczuk, *Prog. Polym. Sci.* **2023**, *139*, 101657.
[38] S. Lowe, N. M. O'Brien-Simpson, L. A. Connal, *Polym. Chem.* **2015**, *6*, 198.
[39] C.-Y. Lee, S.-M. Hu, J. Christy, F.-Y. Chou, T. C. Ramil, H.-Y. Chen, *Adv. Mat. Interf.* **2023**, *10*, 2202286.
[40] L. Yu, C. Schlaich, Y. Hou, J. Zhang, P. L. M. Noeske, R. Haag, *Chemistry* **2018**, *24*, 7742.
[41] P.-Y. J. Yeh, R. K. Kainthan, Y. Zou, M. Chiao, J. N. Kizhakkedathu, *Langmuir* **2008**, *24*, 245.
[42] D. Terada, S. Sotoma, Y. Harada, R. Igarashi, M. Shirakawa, *Bioconjugate Chem.* **2018**, *29*, 2786.
[43] Y. H. Kim, O. W. Webster, *J. Am. Chem. Soc.* **1990**, *112*, 4593.
[44] S. Abbina, S. Vappala, P. Kumar, E. M. J. Siren, C. C. La, U. Abbasi, D. E. Brooks, J. N. Kizhakkedathu, *J. Mater. Chem. B* **2017**, *5*, 9249.
[45] P.-R. Chen, T.-C. Wang, S.-T. Chen, H.-Y. Chen, W.-B. Tsai, *Langmuir* **2017**, *33*, 14657.
[46] M. R. Farani, M. Azarian, H. H. S. Hossein, Z. Abdolvahabi, Z. M. Abgarmi, A. Moradi, S. M. Mousavi, M. Ashrafizadeh, P. Makvandi, M. R. Saeb, N. Rabiee, *ACS Appl. Bio. Mater.* **2022**, *5*, 1305.
[47] J. Xie, S. Qi, Q. Ran, L. Dong, *Materials* **2022**, *15*, 8402.
[48] Y. Deng, J. Saucier-Sawyer, C. Hoimes, J. Zhang, Y.-E. Seo, J. W. Andrejecsk, W. M. Saltzman, *Biomaterials* **2014**, *35*, 6595.
[49] R. K. Kainthan, J. Janzen, E. Levin, D. V. Devine, D. E. Brooks, *Biomacromolecules* **2006**, *7*, 703.
[50] A. Zill, A. L. Rutz, R. E. Kohman, A. M. Alkilany, C. J. Murphy, H. Kong, S. C. Zimmerman, *Chem. Commun.* **2011**, *47*, 1279.
[51] D. Wilms, S. Stiriba, H. Frey, *Acc. Chem. Res.* **2010**, *43*, 129.
[52] A. Sunder, R. Hanselmann, H. Frey, R. Mulhaupt, *Macromolecules* **1999**, *32*, 4240.
[53] E. Moore, B. Delalat, R. Vasani, G. McPhee, H. Thissen, N. H. Voelcker, *ACS Appl. Mater. Interfaces* **2014**, *6*, 15243.
[54] E. Moore, B. Delalat, R. Vasani, H. Thissen, N. H. Voelcker, *Biomacromolecules* **2014**, *15*, 2735.
[55] A. Utrata-Wesolek, W. Walach, J. Aniol, A. L. Sieron, A. Dworak, *Kobunja. Kwahak. Kwa Kisul.* **2016**, *97*, 44.
[56] M. Khan, W. T. S. Huck, *Macromolecules* **2003**, *36*, 5088.
[57] G. Perumal, S. Pappuru, M. Doble, D. Chakraborty, S. Shajahan, M. A. Haija, *ACS Omega* **2023**, *8*, 2377.
[58] A. Boulares-Pender, A. Prager, S. Reichelt, C. Elsner, M. R. Buchmeiser, *J. Appl. Polym. Sci.* **2011**, *121*, 2543.
[59] M. Weinhart, T. Becherer, N. Schnurbusch, K. Schwibbert, H.-J. Kunte, R. Haag, *Adv. Eng. Mater.* **2011**, *13*, B501.
[60] T. Weber, Y. Gies, A. Terfort, *Langmuir* **2012**, *28*, 15916.
[61] Y. He, S. Xing, P. Jiang, Y. Zhao, L. Chen, *Biomacromolecules* **2022**, *23*, 4924.
[62] M. C. Biesinger, L. W. M. Lau, A. R. Gerson, R. S. C. Smart, *Appl. Surf. Sci.* **2010**, *257*, 887.
[63] X. Kong, C. Zeng, X. Wang, J. Huang, C. Li, J. Fei, J. Li, Q. Feng, *Sci. Rep.* **2016**, *6*, 29049.
[64] L. Czuba, *Handbook of Polymer Applications in Medicine and Medical Devices*, Elsevier, Oxford **2014**, p. 9.
[65] G. Beamson, D. Briggs, *High Resolution XPS of Organic Polymers: The Scienta ESCA300 Database*, John Wiley & Sons, Chichester **1992**.
[66] D. Briggs, M. P. Seah, *Practical Surface Analysis: by Auger and X-Ray Photoelecton Spectroscopy*, John Wiley & Sons, Chichester **1983**.

[67] A. P. Ameen, R. J. Ward, R. D. Short, G. Beamson, D. Briggs, *Polymer* **1993**, *34*, 1795.
[68] F. Pippig, S. Sarghini, A. Holländer, S. Paulussen, H. Terryn, *Surf. Interface Anal.* **2009**, *41*, 421.
[69] J.-C. Ruiz, S. Taheri, A. Michelmore, D. E. Robinson, R. D. Short, K. Vasilev, R. Förch, *Plasma Processes Polym.* **2014**, *11*, 888.
[70] J. Wouw, J. Joles, *Clin. Kid J.* **2022**, *15*, 624.
[71] T. A. Horbett, *J. Biomed. Mater. Res. A* **2018**, *106*, 2777.
[72] Y. J. Wu, A. J. Griggs, J. S. Jen, S. Manolache, F. S. Denes, R. B. Timmons, *Plasmas Polym.* **2001**, *6*, 123.
[73] Y. J. Wu, R. B. Timmons, J. S. Jen, F. E. Molock, *Colloids Surf., B* **2000**, *18*, 235.
[74] M. S. Wagner, S. L. McArthur, M. Shen, T. A. Horbett, D. G. Castner, *J. Biomater. Sci. Polym. Ed.* **2002**, *13*, 407.
[75] X. Liu, L. Yuan, D. Li, Z. Tang, Y. Wang, G. Chen, H. Chen, J. L. Brash, *J. Mater. Chem. B* **2014**, *2*, 5718.
[76] W.-B. Tsai, J. M. Grunkemeier, C. D. McFarland, T. A. Horbett, *J. Biomed. Mater. Res.* **2002**, *60*, 348.
[77] A. G. Shard, R. Havelund, S. J. Spencer, I. S. Gilmore, M. R. Alexander, T. B. Angerer, S. Aoyagi, J.-P. Barnes, A. Benayad, A. Bernasik, G. Ceccone, J. D. P. Counsell, C. Deeks, J. S. Fletcher, D. J. Graham, C. Heuser, T. G. Lee, C. Marie, M. M. Marzec, G. Mishra, D. Rading, O. Renault, D. J. Scurr, H. K. Shon, V. Spampinato, H. Tian, F. Wang, N. Winograd, K. Wu, et al., *J. Phys. Chem. B* **2015**, *119*, 10784.
[78] L. C. S. Antunes, P. Visca, K. J. Towner, *Pathog. Dis.* **2014**, *71*, 292.
[79] K. Harika, V. P. Shenoy, N. Narasimhaswamy, K. Chawla, *J. Glob. Infect. Dis.* **2020**, *12*, 129.
[80] A. R. Crisp, B. Short, R. Rowan, G. Ramage, I. U. R. Rehman, R. D. Short, C. Williams, *Biofilm* **2023**, *6*, 100141.
[81] J. E. Aslan, A. Itakura, J. M. Gertz, O. J. T. McCarty, in *Platelets and Megakaryocytes, Additional Protocols and Perspectives*, (Ed: J. M. M.-S. M. Gibbins), Springer, New York **2012**, Vol. *3*, p. 91.
[82] D. Lee, K. P. Fong, M. R. King, L. F. Brass, D. A. Hammer, *Biophys. J.* **2012**, *102*, 472.
[83] D. C. Leslie, A. Waterhouse, J. B. Berthet, T. M. Valentin, A. L. Watters, A. Jain, P. Kim, B. D. Hatton, A. Nedder, K. Donovan, E. H. Super, C. Howell, C. P. Johnson, T. L. Vu, D. E. Bolgen, S. Rifai, A. R. Hansen, M. Aizenberg, M. Super, J. Aizenberg, D. E. Ingber, *Nat. Biotechnol.* **2014**, *32*, 1134.
[84] Y. Qiu, A. C. Brown, D. R. Myers, Y. Sakurai, R. G. Mannino, R. Tran, B. Ahn, E. T. Hardy, M. F. Kee, S. Kumar, G. Bao, T. H. Barker, W. A. Lam, *Proc. Natl. Acad. Sci. USA* **2014**, *111*, 14430.
[85] S. Sheth, F. Litvack, V. Dev, M. C. Fishbein, J. S. Forrester, N. Eigler, *Circulation* **1996**, *94*, 1733.
[86] A. B. Chandler, *Lab Invest.* **1958**, *7*, 110.
[87] W. Zhang, P. Li, B. Neumann, H. Haag, M. Li, Z. Xu, C. Zhou, L. Scheideler, H.-P. Wendel, H. Zhang, J. Geis-Gerstorfer, G. Wan, *Mater. Sci. Eng., C* **2021**, *119*, 111594.
[88] J. Ng, C. V. Bourantas, R. Torii, H. Y. Ang, E. Tenekecioglu, P. W. Serruys, N. Foin, *Arterioscler. Thromb. Vasc. Biol.* **2017**, *37*, 2231.
[89] Z. A. Ali, N. J. Alp, H. Lupton, N. Arnold, T. Bannister, Y. Hu, S. Mussa, M. Wheatcroft, D. R. Greaves, J. Gunn, K. M. Channon, *Arterioscler. Thromb. Vasc. Biol.* **2007**, *27*, 833.
[90] R. K. Kainthan, D. E. Brooks, *Biomaterials* **2007**, *28*, 4779.
[91] R. K. Kainthan, S. R. Hester, E. Levin, D. V. Devine, D. E. Brooks, *Biomaterials* **2007**, *28*, 4581.
[92] R. Chapanian, I. Constantinescu, D. E. Brooks, M. D. Scott, J. N. Kizhakkedathu, *Biomaterials* **2012**, *33*, 3047.
[93] M. W. Kulka, C. Nie, P. Nickl, Y. Kerkhoff, A. Garg, D. Salz, J. Radnik, I. Grunwald, R. Haag, *Adv. Mater. Interfaces* **2020**, *7*, 2000931.
[94] Q. Wei, T. Becherer, R. C. Mutihac, P. L. Noeske, F. Paulus, R. Haag, I. Grunwald, *Biomacromolecules* **2014**, *15*, 3061.
[95] F. J. Schoen, A. S. Hoffman, in *Biomaterials Science*, (3rd ed.), (Eds: B. D. Ratner, A. S. Hoffman, F. J. Schoen, J. E. Lemons), Academic Press, Oxford **2013**, p. 1361.
[96] M. Noris, G. Remuzzi, *Semin. Nephrol.* **2013**, *33*, 479.
[97] G. T. Nguyen, E. R. Green, J. Mecsas, *Front. Cell Infect. Microbiol.* **2017**, *7*, 373.
[98] B. Uttara, A. V. Singh, P. Zamboni, R. T. Mahajan, *Curr. Neuropharmacol.* **2009**, *7*, 65.
[99] A. J. Kattoor, N. V. K. Pothineni, D. Palagiri, J. L. Mehta, *Curr. Atheroscler. Rep.* **2017**, *19*, 42.
[100] R. T. Hannan, S. M. Peirce, T. H. Barker, *ACS Biomater. Sci. Eng.* **2018**, *4*, 1223.
[101] F. Heymann, K. T. von Trotha, C. Preisinger, P. Lynen-Jansen, A. A. Roeth, M. Geiger, L. J. Geisler, A. K. Frank, J. Conze, T. Luedde, C. Trautwein, M. Binnebösel, U. P. Neumann, F. Tacke, *JCI Insight* **2019**, *4*, e123862.
[102] B. H. Shin, B. H. Kim, S. Kim, K. Lee, Y. B. Choy, C. Y. Heo, *Biomater. Res.* **2018**, *22*, 37.
[103] M. Jafari, S. S. Abolmaali, H. Najafi, A. M. Tamaddon, *Int. J. Pharm.* **2020**, *576*, 118959.
[104] A. M. Cherian, S. V. Nair, V. Maniyal, D. Menon, *APL Bioeng.* **2021**, *5*, 021508.
[105] D. G. Kokkinidis, E. J. Armstrong, *J. Thorac. Dis.* **2020**, *12*, 1681.
[106] E. Moore, H. Thissen, N. H. Voelcker, *Prog. Surf. Sci.* **2013**, *88*, 213.
[107] R. Suchentrunk, H. J. Fuesser, G. Staudigl, D. Jonke, M. Meyer, *Surf. Coat. Technol.* **1999**, *112*, 351.
[108] C. Hopkins, C. A. Sweeney, C. O'Connor, P. E. McHugh, J. P. McGarry, *Ann. Biomed. Eng.* **2016**, *44*, 419.
[109] H. J. Griesser, *Vacuum* **1989**, *39*, 485.
[110] J.-P. Cazenave, P. Ohlmann, D. Cassel, A. Eckly, B. Hechler, C. Gachet, in *Platelets and Megakaryocytes*, (Eds: J. M. Gibbins, M. P. Mahaut-Smith), Humana Press, Totowa, NJ, **2004**, Vol. *1*, pp. 13–28.
[111] Z. A. Ali, C. A. Bursill, Y. Hu, R. P. Choudhury, Q. Xu, D. R. Greaves, K. M. Channon, *Circulation* **2005**, *112*, I235.